

Hydrology

SANDIA REPORT SAND84-0192 • Unlimited Release • UC-70
Printed September 1984

Effect of Host-Rock Dissolution and Precipitation on Permeability in a Nuclear Waste Repository in Tuff

Jeffrey W. Braithwaite, Francis B. Nimick

Prepared by
Sandia National Laboratories
Albuquerque, New Mexico 87185 and Livermore, California 94550
for the United States Department of Energy
under Contract DE-AC04-76DP00789

HYDROLOGY DOCUMENT NUMBER 140
(8/84) HL1002198
HL1002198

SAND84-0192

Unlimited Release
Printed September 1984

EFFECT OF HOST-ROCK DISSOLUTION AND PRECIPITATION ON
PERMEABILITY IN A NUCLEAR WASTE REPOSITORY IN TUFF

by

Jeffrey W. Braithwaite
NNWSI Repository Performance Assessments Division 6312

and

Francis B. Nimick
NNWSI Geotechnical Projects Division 6313

Sandia National Laboratories
Albuquerque, New Mexico 87185

ABSTRACT

A study has been conducted to determine whether thermally induced, host-rock mineral dissolution and precipitation processes could decrease the isolation capability of a potential high-level nuclear waste repository in tuff by significantly altering the permeability of the formation. Conservative assumptions were used that maximized the predicted quantity of rock dissolution and precipitation. Porosity changes were calculated as a function of time, depth, emplaced waste power density, and water flux for both matrix and fracture flow. Cumulative porosity changes were shown to be very small, and net decreases in porosity were shown to occur only in the vicinity of the repository horizon if the groundwater vaporizes. The differences in permeability for both matrix and fracture flow resulting from these small cumulative porosity changes should have no significant effect on the overall hydrologic patterns at the site at Yucca Mountain, Nevada.

TABLE OF CONTENTS

	<u>Page</u>
Introduction	1
Approach	3
Identification of the Controlling Mineralogy	3
Environmental Effects on Amorphous Silica Solubility	7
Temperature Distribution	8
Model	14
Results for Constant Porosity	20
Effect of time	20
Effect of Initial Matrix Porosity	24
Effect of Percolation Rate and Pore Saturation	26
Effect of Areal Power Density	26
Effect of Water Vaporization	26
Results for Variable Matrix Porosity	32
Results for Permeability Changes	35
Matrix Flow	37
Fracture Flow	37
Summary	41
References	44

LIST OF FIGURES

		<u>Page</u>
Figure 1.	Comparison of stratigraphic and functional units in tuffs in the unsaturated zone at Yucca Mountain.	4
Figure 2.	Temperature distribution for a proposed repository at Yucca Mountain containing 57 kW/acre spent fuel.	10
Figure 3.	Temperature distribution for a proposed repository at Yucca Mountain containing 90 kW/acre spent fuel.	11
Figure 4.	Schematic diagram of the block or grid structure used in the mineral dissolution and precipitation model.	17
Figure 5.	Cumulative matrix porosity change as a function of depth and time for a 57 kW/acre spent fuel repository contained in tuff with a single initial matrix porosity of 0.12, a constant percolation rate of 0.5 mm/yr, and no vaporization.	21
Figure 6.	Cumulative matrix porosity change as a function of time at the depth of the repository for a 57 kW/acre loading in tuff with a single initial matrix porosity of 0.12, a constant percolation rate of 0.5 mm/yr, and no water vaporization.	23
Figure 7.	Cumulative matrix porosity change as a function of depth and initial matrix porosity at 250 years and a percolation rate of 0.5 mm/yr for a 57 kW/acre spent fuel repository.	25
Figure 8.	Cumulative matrix porosity change as a function of depth, percolation rate, and saturation for a 57 kW/acre spent fuel repository with a single initial matrix porosity of 0.12 at 250 years following emplacement and no water vaporization.	27
Figure 9.	Cumulative matrix porosity change as a function of depth for the two area power densities considered and a single initial matrix porosity of 0.12, a percolation rate of 0.5 mm/yr, no water vaporization, and at 10,000 years following emplacement.	28

LIST OF FIGURES
(cont'd.)

	<u>Page</u>
Figure 10. Cumulative matrix porosity change as a function of depth and time for a 57 kW/acre spent fuel repository with a single initial matrix porosity of 0.12, a constant percolation rate of 0.5 mm/yr, and water vaporization for regions in which the temperature exceeded 100°C.	29
Figure 11. Cumulative matrix porosity change as a function of depth with and without water vaporization for a 57 kW/acre spent fuel repository with a single initial matrix porosity of 0.12, and a constant percolation rate of 0.5 mm/yr.	30
Figure 12. Cumulative matrix porosity change as a function of depth for the two areal power densities considered and a single initial matrix porosity of 0.12, a percolation rate of 0.5 mm/yr, water vaporization, and at 10,000 years following emplacement.	31
Figure 13. Cumulative matrix porosity change as a function of depth and time for a 57 kW/acre spent fuel repository using the initial matrix porosity of each stratigraphic unit, a constant percolation rate of 0.5 mm/yr, and water vaporization.	33
Figure 14. Cumulative matrix porosity change as a function of depth and time for a 90 kW/acre spent fuel repository using the initial matrix porosity of each stratigraphic unit, a constant percolation rate of 0.5 mm/yr, and water vaporization.	34
Figure 15. Cumulative matrix porosity change as a function of depth and percolation rate for a 57 kW/acre spent fuel repository using the initial matrix porosity of each stratigraphic unit, and water vaporization.	36
Figure 16. Comparison of the cumulative porosity changes in the matrix and the fractures of the Topopah Spring Member at 250 years after the emplacement of a 57 kW/acre spent fuel repository beneath Yucca Mountain.	40

LIST OF TABLES

		<u>Page</u>
Table 1.	Temperature distribution as a function of time and depth for a hypothetical repository at Yucca Mountain containing 57 kW/acre spent fuel (temperatures calculated at times from 250 to 10,000 years after emplacement).	12
Table 2.	Temperature distribution as a function of time and depth for a hypothetical repository at Yucca Mountain containing 90 kW/acre spent fuel (temperatures calculated at times from 250 to 10,000 years after emplacement).	13
Table 3.	Definition and relevant properties for the six stratigraphic units considered.	15
Table 4.	Cumulative porosity change as a function of time and position for a hypothetical repository at Yucca Mountain (calculated at time from 250 to 10,000 years after emplacement).	22

INTRODUCTION

The Nevada Nuclear Waste Storage Investigations (NNWSI) project is studying the feasibility of locating a licensed repository for high-level radioactive waste on or near the Nevada Test Site (NTS) in southern Nevada. Currently, the project is evaluating a tuff site in the unsaturated zone at Yucca Mountain in and near the southwest part of the NTS.

The task of assessing the performance of the overall waste-isolation system at Yucca Mountain is being performed at Sandia National Laboratories. One initial function of this performance assessment effort is to participate in the determination of whether the proposed site satisfies the isolation-related DOE siting guidelines. A potentially adverse condition in the Rock Characteristics section of the Siting Guidelines (960.4-2-3) is the following (U.S. Department of Energy, 1984):

"A combination of geologic structure, geochemical and thermal properties, and hydrologic conditions in the host rock and surrounding units such that the heat generated by the waste could significantly decrease the isolation provided by the host rock as compared with the pre-waste emplacement conditions."

In the analysis of this condition, several potential heat-related effects on the isolation characteristics of the host rock were identified and studied. One of these effects is permeability change due to host-rock dissolution and precipitation processes. Although it was recognized that the minerals composing the tuff have very limited solubilities in groundwater and that evidence of significant aqueous dissolution is not present in this region (Heiken and Bevier, 1979), the potential exists for altering the permeability because of a small quantity of thermally-induced rock dissolution and deposition. The results of an investigation of this potential hydrological alteration are presented in this report.

The portion of Yucca Mountain that lies in the unsaturated zone (approximately the top 500-600 m) consists of alternating layers of densely welded and nonwelded tuff. As a basis for this analysis, the repository horizon was assumed to be at a constant depth below the surface of 390 m. This hypothetical repository would be contained in a thick ash-flow section of the Topopah Spring unit that is densely welded, relatively nonporous, highly fractured, and highly transmissive. Below this layer is a relatively thin, densely welded vitric layer, underlain by a thick interval of nonwelded, highly porous, but relatively unfractured and nontransmissive argillic and zeolitic bedded and ash-flow tuffs.

Recent water-flow studies conducted at Sandia have shown that water probably flows through the pores of the densely welded tuff layer at very low fluxes (less than 1 mm/yr), and that, primarily because of the presence of fractures, the bulk permeability of the various tuff layers is higher than the water flux (Peters and Gauthier, 1984). It is important to note that, if matrix flow occurs at 0.5 mm/yr, the groundwater will only travel through approximately 40 m of the Topopah Spring unit in 10,000 yr. Thus, although water flow is explicitly treated in this study, the flow is actually almost negligible.

The heating and subsequent cooling of groundwater as it percolates vertically down through the host rock and past the radioactive waste could induce host-rock dissolution and precipitation, which, in turn, could change the local permeability of the tuff layers. Currently, the magnitude of either increases or decreases in permeability which would adversely affect isolation have not been identified. Since the transmissivity of the tuff layers appears to be sufficient to allow all of the incoming water to flow through without saturating the formation, any net rock dissolution would only further increase the transmissivity and thus should have a negligible impact on water flow characteristics. However, decreases in permeability due to mineral precipitation could potentially affect the isolation characteristics of the host rock by causing the rock to saturate. Saturation of the rock could increase the quantity and contact time of water with the waste package and could induce fracture flow. These two changes could potentially increase radionuclide release rates from the waste package and decrease radionuclide

travel time. After consideration of these factors, the most important aspect of this study was to determine whether any significant decreases in permeability could occur.

APPROACH

A precise determination of the quantity of rock that would dissolve, be transported, and subsequently precipitate would require detailed knowledge of temperature distributions, groundwater chemistry, groundwater flow characteristics, and reaction kinetics of all the relevant minerals. Since such detailed information is not available, the approach used in this study was to bound the effect on permeability by using assumptions that lead to conservatively high estimates of matrix and fracture porosity changes. These porosity change predictions can then be used to calculate new matrix and fracture permeabilities. In the remainder of this section, the types and sources of information used in this conservative study are given along with any required justification. This information has been divided into three subsections: 1) identification of the controlling mineralogy, 2) environmental effects on amorphous silica solubility, and 3) temperature distribution.

Identification of the Controlling Mineralogy

As presently envisioned, the repository at Yucca Mountain would be constructed in the lower part of the thick (43 to 190 m) densely welded part of the Topopah Spring Member of the Paintbrush Tuff (Unit IIB in Figure 1). This unit is composed primarily of alkali and plagioclase feldspars and several forms of silica which include quartz, cristobalite, and tridymite. Minor mineralogic constituents include mica, clay, and Fe-Ti oxides. Detailed descriptions of the mineralogy are contained in Heiken and Bevier, 1979; Sykes et al., 1979; Carroll et al., 1981; Bish et al., 1982; Broxton et al., 1982; and Caporuscio et al., 1982.

The analysis of the dissolution and precipitation of minerals contained within Yucca Mountain was simplified by assuming that the groundwater always maintains saturation with respect to amorphous silica. That is, the quantity of material transferred between the groundwater and the rock can be followed by calculating thermally-induced changes in amorphous silica solubility. This approach is justified for the following reasons:

	Stratigraphic Unit	Functional Unit ¹	Thickness of Stratigraphic Unit (m)
	Tiva Canyon	IA2	0->129
	Yucca Mountain & Pah Canyon	IB	0-110
Repository Horizon	Topopah Spring	IIA	301-360
		IIB	
		IIIA	
	Calico Hills	IIIB	IVA

1 — See Nimick (1984)

Figure 1. Comparison of stratigraphic and functional units in tuffs in the unsaturated zone at Yucca Mountain.

1. The mineralogy can be described as consisting of two major phases: the feldspars and the silica polymorphs (e.g., quartz, cristobalite, amorphous silica). The quantity of these phases that will dissolve depends on the groundwater chemistry, the temperature and pressure, leach kinetics, and the amount of reaction time. As shown, for example, by Morey et al., 1962; Siever, 1962; and Rimstidt and Barnes, 1980, the kinetics of some silica reactions are so slow that equilibrium with a solution is thought to be unattainable on a laboratory time scale. However, from a dissolution standpoint, assuming that equilibrium can be achieved allows one to estimate the maximum quantity of material that can be dissolved for a given temperature, pressure, and solution composition.

2. Some published descriptions of sandstones that have undergone diagenesis and/or pressure solution suggest that quartz is more susceptible to dissolution and precipitation than are feldspars (Heald, 1965; deBoer et al., 1977; Heald and Baker, 1977). Other investigators have observed strong dissolution of both feldspars and quartz (Morris et al., 1979; Tardy and Cassan, 1981). Additionally, examination of published data on the concentration of silica in waters equilibrated with amorphous silica at room temperature and pressure show a range of 0.0013 to 0.0078 mole/l (from data given by Siever, 1962; Marshall, 1980; Willey, 1980). Under similar conditions, silica concentrations in equilibrium with feldspar range from 0.00002 to 0.0006 mole/l (from data given by Wollast, 1967; Huang and Kiang, 1972). Thus, the amorphous-silica assumption is more conservative than an assumption that the groundwater maintains saturation with respect to the feldspars, since feldspars must precipitate whenever the silica concentration exceeds 0.0006 mole/l.

3. During dissolution, the feldspars release variable amounts of potassium, sodium, calcium, aluminum, and silicon. The silica polymorphs contribute only silicon to the groundwater. Therefore, a comparison was made between the quantity of rock dissolved experimentally under isothermal conditions and a prediction using the amorphous silica assumption under similar conditions. In rock-water interaction tests conducted at the Lawrence

Livermore National Laboratory, wafers of Topopah Spring core were submerged in representative groundwater and heated to 150°C for varied periods of time up to a month. Most of the weight loss occurred in the first two weeks. The weight loss observed after one month was 1.4 percent. The weight loss calculated for similar conditions using the amorphous silica solubility equation (see the discussion of the model later in this paper) was 1.8 percent. This result demonstrates that the model is sufficiently conservative to account for the dissolution of non-silica components while still providing results that are reasonable with respect to the general level of dissolution observed experimentally.

4. Numerous experimental studies (e.g., those by Kennedy, 1950; Morey et al., 1962; Crerar and Anderson, 1971; Fournier, 1977) have shown that the solubility of amorphous silica is approximately two to four times that of cristobalite and four to nineteen times that of quartz for temperatures up to 200°C.

A description of the behavior of cristobalite or tridymite during diagenesis was not found. However, it is probably safe to assume that cristobalite, as a metastable phase at low temperature (Sosman, 1965), will dissolve faster than quartz. Since cristobalite dissolution will involve loss of a larger volume of solid than will quartz dissolution for a given quantity of dissolved silica, cristobalite was assumed to be the source of the silica in the groundwater.

Observations of outcrops and drill hole core from Yucca Mountain suggest that opaline silica has precipitated from groundwater in the tuffs at some time in the geologic past. This silica phase was assumed to be close to amorphous silica in density, and the latter was used as the phase that precipitates from solution in this study.

To summarize, the following assumptions concerning the processes controlling host-rock dissolution and precipitation were used in this analysis (the upper bound each assumption provides is given in parentheses):

1. Silica concentrations in groundwater are determined by equilibrium saturation with amorphous silica (mass of rock dissolving and subsequently precipitating).
2. Cristobalite is the solid phase contributing most of the silica to the groundwater (volume of silica dissolving).
3. Amorphous silica is the solid phase precipitating from cooling groundwater (volume of silica precipitating).

These three bounding assumptions produced conservative results in that the potential for reducing permeability beneath the repository horizon is maximized.

Environmental Effects on Amorphous Silica Solubility

Several studies have found that the presence of moderate quantities of cations such as sodium, potassium, calcium, and magnesium either has no effect or decreases amorphous silica solubility (e.g., Nash and Marshall, 1956; van Lier et al., 1960; Fournier and Rowe, 1966; Nikitina, 1976; Marshall and Warakomski, 1980). Siever (1962) determined that solubility in brines with up to 50,000 ppm dissolved solids was little different from the solubility in distilled water. Reardon (1979) found that at very low pH values, the presence of ferric iron enhanced silica solubility through complexing. However, groundwaters at Yucca Mountain have neither significant concentrations of ferric iron nor pH values as low as those at which the aqueous complex would be stable.

Silica solubility is not affected significantly by changes in pH at moderate values of pH (4 to 9). Both Crerar and Anderson (1971) and Nikitina (1976) found a slight increase in solubility with increasing pH, while Siever (1962) found no effect at all for a pH range of 2 to 9.5.

The effects of pressure and temperature on solubility have been studied extensively. All the studies have shown that silica concentrations in water increase with increasing temperature, whether the dissolving solid is quartz (Mosebach, 1957; Siever, 1962; Walther and Helgeson, 1977), silica glass (Mosebach, 1957), silica gel (Volosov et al., 1972), amorphous silica

(Mosebach, 1957, Siever, 1962), or granite (Holley et al., 1980). Two studies make explicit statements about the effect of pressure. Mosebach (1957) found that pressure has a negligible effect on solubility, while Siever (1962) suggested a slight increase in solubility with increasing pressure.

Temperature Distribution

The dissolution and precipitation of the host rock is driven by temperature changes produced by the emplacement and decay of several radionuclides contained in the high-level wastes. Of the two waste-forms currently being considered, spent fuel contains the larger quantity of heat-generating radionuclides. The higher integrated heat load will produce larger temperature changes and therefore the greatest amount of dissolution and precipitation. For these reasons, spent fuel was selected as the waste form to use in this evaluation.

A thermomechanical study was recently completed in which the temperature distribution as a function of time along the vertical centerline intersecting the repository area was predicted for two different areal power densities: the current reference of 57-kW/acre (14 W/m^2) and a higher loading of 90-kW/acre (22 W/m^2) (Svalstad, 1984). This far-field analysis assumed that the spent fuel was uniformly distributed throughout the repository (in a narrow flat disk) at a depth of 390 m below the surface. The use of the temperature distribution along the centerline is again a conservative approach since it includes both the maximum absolute temperatures and the maximum temperature gradient.

The temperature distributions given in Svalstad (1984) for a number of specific times following emplacement were then fit with a series of linear and exponential functions. For example, at 1000 years and a power density of 57 kW/acre (14 W/m^2), the following equations were used to predict the temperature as a function of depth:

Baseline (geothermal gradient):

$$T = 13.2 + 0.031 * \text{Depth} \quad (1)$$

For depth < 390 m:

$$T = 18.47 * \exp(0.004 * \text{Depth}); \quad (2)$$

For depth > 390 m:

$$T = 297.24 * \exp(-0.003 * \text{Depth}); \quad (3)$$

and the temperature at 390 m is 99.9°C.

T is in °C and depth is in meters. The temperatures calculated using equations (2) and (3) were constrained to be not less than the baseline temperature or greater than the 390-m maximum temperature.

Temperature data required in the analysis for times other than those for which Svalstad (1984) provided distributions were calculated by linearly interpolating between data based on existing distributions. Examples of the resultant temperature profiles for both power densities considered are shown graphically in Figures 2 and 3 and in tabular form in Tables 1 and 2. Depths to only 600 m were considered because that is the approximate depth of the water table. At and below the water table where the formations are already saturated, permeability changes are not as important. Additionally, changes in the thermal gradient are quite small at these depths. Times to 10,000 years were used because that is the length of time for which the EPA (in 10 CFR 191) requires calculations of the effectiveness of isolation.

As shown in Figures 2 and 3, some portions of the rock will heat up for some time to temperatures that exceed 100°C. Since the proposed repository would be in a highly fractured, unsaturated zone, atmospheric pressure will not, in general, be exceeded. Therefore, the water in these high temperature regions could vaporize, and the rock could dry out (Pruess and Wang, 1983). The existence of a dry-out zone also depends on other properties of the rock such as permeability and capillary pressures. In some of the evaluations conducted in this study, water vaporization was included to determine whether the precipitation of the solids initially dissolved in the water because of the geothermal gradient could cause a significant decrease in permeability.

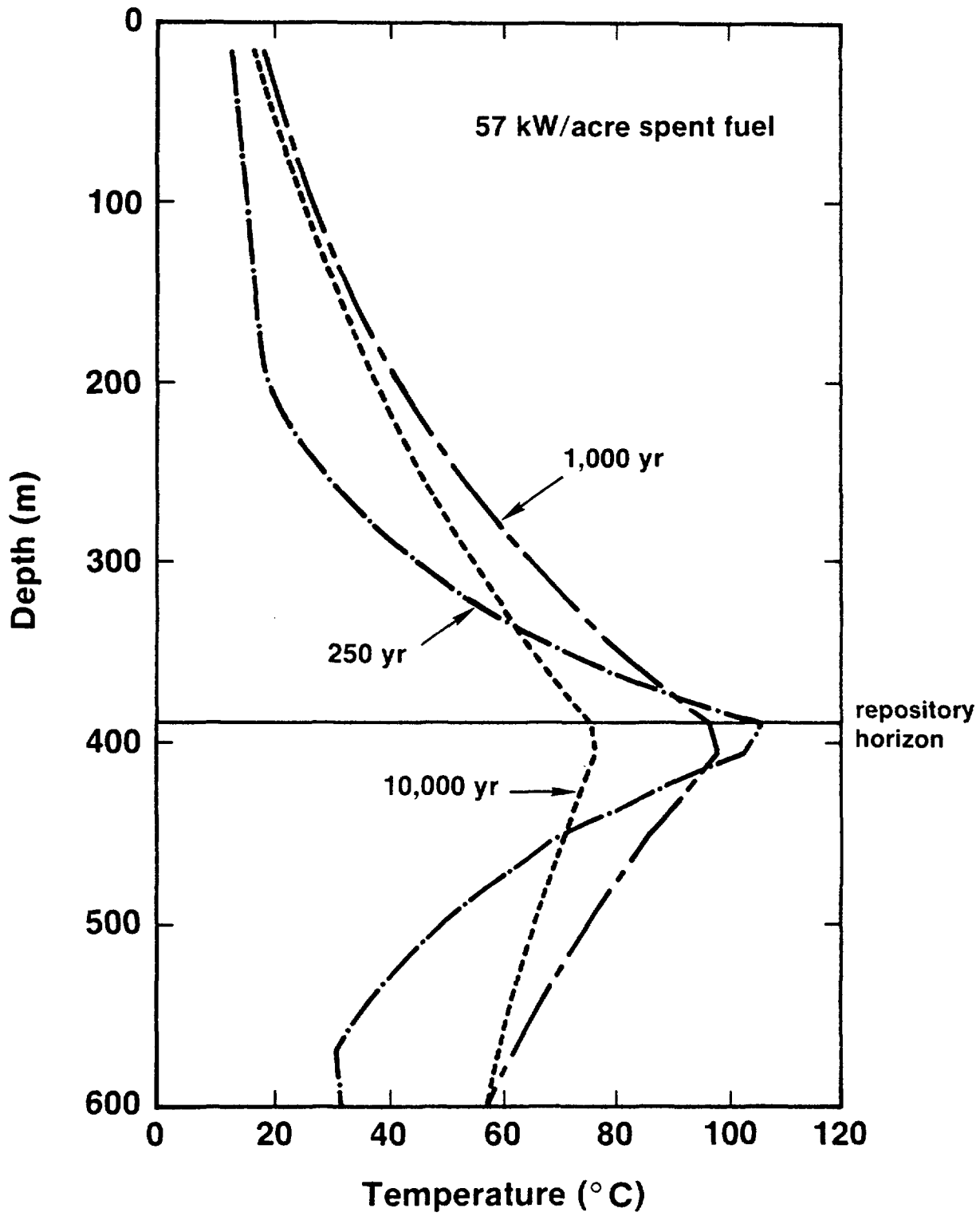


Figure 2. Temperature distribution for a proposed repository at Yucca Mountain containing 57 kW/acre spent fuel. The repository horizon is at 390 meters.

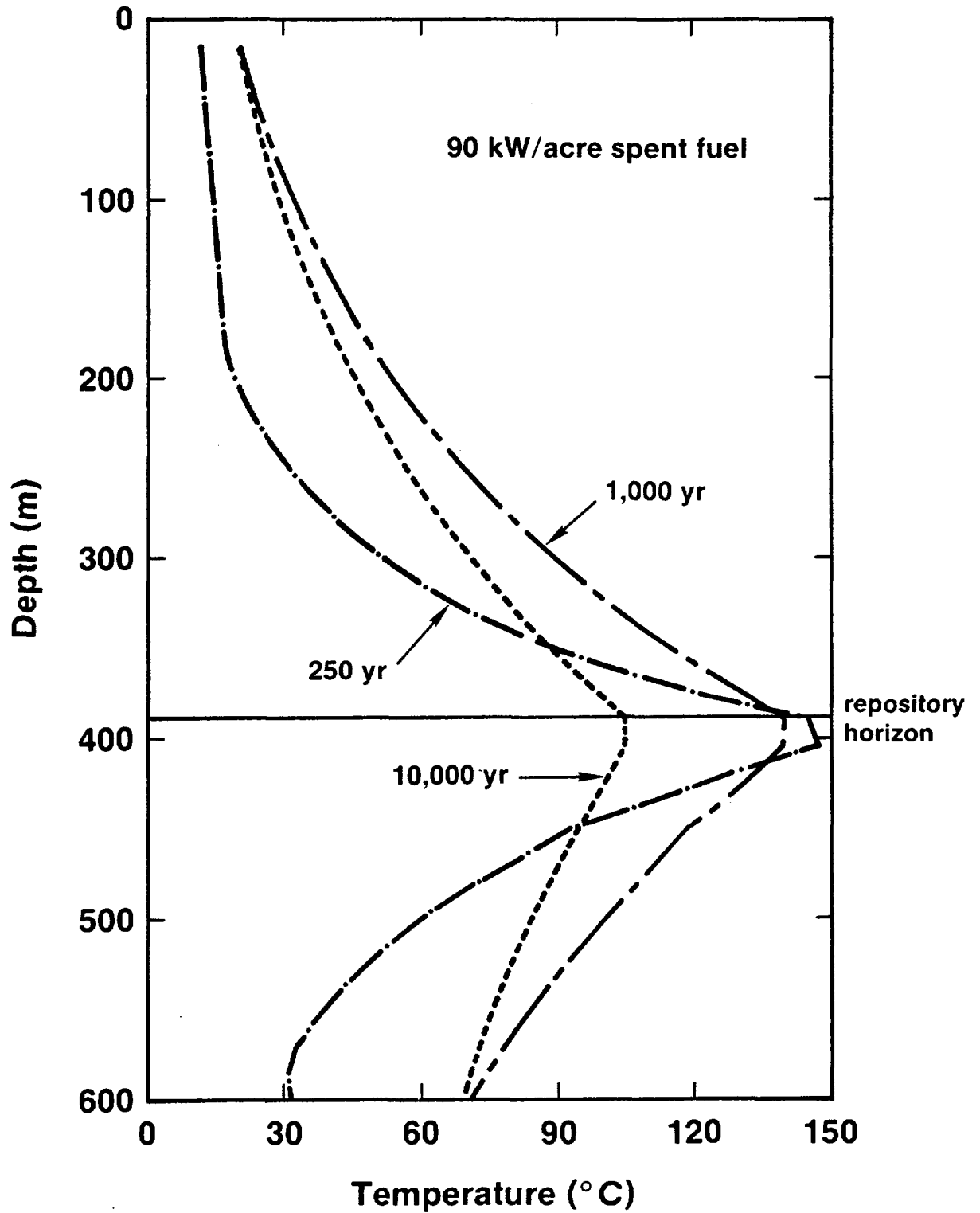


Figure 3. Temperature distribution for a proposed repository at Yucca Mountain containing 90 kW/acre spent fuel.

Table 1. Temperature distribution as a function of time and depth for a hypothetical repository at Yucca Mountain containing 57 kW/acre spent fuel (temperatures calculated at times from 250 to 10,000 years after emplacement).

Depth (m)	Temperature (°C)									
	250	500	1000	1500	2000	3000	4000	6000	8000	10000
15.	13.	13.	19.	19.	19.	19.	18.	18.	18.	17.
30.	14.	14.	20.	20.	20.	20.	20.	19.	19.	19.
45.	14.	14.	22.	22.	22.	21.	21.	21.	20.	20.
60.	15.	15.	23.	23.	23.	23.	23.	22.	22.	22.
75.	15.	16.	25.	25.	25.	24.	24.	24.	23.	23.
90.	16.	18.	26.	26.	26.	26.	26.	25.	25.	25.
105.	16.	20.	28.	28.	28.	28.	28.	27.	27.	26.
120.	17.	21.	30.	30.	30.	30.	29.	29.	28.	28.
135.	17.	23.	32.	32.	32.	32.	31.	31.	30.	30.
150.	18.	26.	34.	34.	34.	34.	33.	33.	32.	32.
165.	18.	28.	37.	36.	36.	36.	36.	35.	34.	34.
180.	19.	31.	39.	39.	39.	38.	38.	37.	36.	36.
195.	19.	33.	42.	41.	41.	41.	40.	39.	39.	38.
210.	21.	37.	44.	44.	44.	43.	43.	42.	41.	40.
225.	24.	40.	47.	47.	47.	46.	46.	44.	43.	42.
240.	27.	44.	51.	50.	50.	49.	48.	47.	46.	44.
255.	31.	48.	54.	54.	53.	52.	52.	50.	49.	47.
270.	35.	52.	58.	57.	57.	56.	55.	53.	51.	50.
285.	40.	57.	61.	61.	60.	59.	58.	56.	54.	52.
300.	45.	62.	65.	65.	64.	63.	62.	60.	58.	55.
315.	52.	68.	70.	69.	69.	67.	66.	63.	61.	58.
330.	60.	74.	75.	74.	73.	72.	70.	67.	64.	61.
345.	69.	81.	80.	79.	78.	76.	75.	71.	68.	65.
360.	79.	89.	85.	84.	83.	81.	79.	76.	72.	68.
375.	91.	97.	91.	90.	89.	87.	84.	80.	76.	72.
390.	105.	106.	97.	96.	94.	92.	90.	85.	81.	76.
405.	102.	105.	98.	97.	95.	93.	91.	86.	81.	77.
420.	91.	98.	94.	93.	92.	90.	87.	83.	79.	75.
435.	80.	92.	90.	89.	88.	86.	84.	80.	77.	73.
450.	71.	86.	86.	85.	85.	83.	81.	78.	74.	71.
465.	64.	80.	83.	82.	81.	80.	78.	75.	72.	69.
480.	57.	75.	79.	79.	78.	77.	75.	73.	70.	68.
495.	51.	71.	76.	76.	75.	74.	73.	71.	68.	66.
510.	46.	66.	73.	73.	72.	71.	70.	68.	66.	65.
525.	41.	62.	70.	70.	69.	68.	68.	66.	65.	63.
540.	37.	58.	67.	67.	67.	66.	65.	64.	63.	62.
555.	33.	54.	64.	64.	64.	63.	63.	62.	61.	60.
570.	31.	51.	62.	62.	61.	61.	61.	60.	60.	59.
585.	31.	48.	59.	59.	59.	59.	59.	59.	58.	58.
600.	32.	45.	57.	57.	57.	57.	57.	57.	57.	57.

Table 2. Temperature distribution as a function of time and depth for a hypothetical repository at Yucca Mountain containing 90 kW/acre spent fuel (temperatures calculated at times from 250 to 10,000 years after emplacement).

Depth (m)	Temperature (°C)									
	250	500	1000	1500	2000	3000	4000	6000	8000	10000
15.	13.	13.	22.	22.	22.	22.	22.	22.	22.	22.
30.	14.	14.	24.	24.	24.	24.	23.	23.	23.	23.
45.	14.	16.	26.	26.	25.	25.	25.	25.	25.	24.
60.	15.	17.	28.	27.	27.	27.	27.	27.	26.	26.
75.	15.	19.	30.	30.	29.	29.	29.	29.	28.	28.
90.	16.	21.	32.	32.	32.	31.	31.	31.	30.	29.
105.	16.	23.	34.	34.	34.	34.	33.	33.	32.	31.
120.	17.	26.	37.	37.	37.	36.	36.	35.	34.	33.
135.	17.	28.	40.	40.	39.	39.	38.	37.	37.	36.
150.	18.	31.	43.	43.	42.	42.	41.	40.	39.	38.
165.	18.	34.	46.	46.	46.	45.	44.	43.	42.	40.
180.	19.	38.	50.	49.	49.	48.	48.	46.	45.	43.
195.	20.	41.	54.	53.	53.	52.	51.	49.	48.	46.
210.	23.	46.	58.	57.	57.	56.	55.	53.	51.	49.
225.	26.	50.	62.	62.	61.	60.	59.	57.	54.	52.
240.	29.	55.	67.	66.	66.	64.	63.	61.	58.	56.
255.	34.	61.	72.	72.	71.	69.	68.	65.	62.	59.
270.	39.	67.	78.	77.	76.	75.	73.	70.	66.	63.
285.	45.	74.	84.	83.	82.	80.	78.	75.	71.	67.
300.	53.	81.	90.	89.	88.	86.	84.	80.	76.	72.
315.	62.	89.	97.	96.	95.	93.	90.	86.	81.	77.
330.	72.	98.	105.	103.	102.	100.	97.	92.	87.	82.
345.	86.	108.	113.	111.	110.	107.	104.	99.	93.	88.
360.	101.	119.	121.	120.	118.	115.	112.	106.	100.	94.
375.	121.	131.	131.	129.	127.	124.	120.	114.	107.	100.
390.	145.	144.	140.	138.	136.	132.	129.	121.	113.	105.
405.	147.	150.	140.	138.	136.	132.	128.	121.	113.	105.
420.	126.	138.	133.	131.	129.	126.	122.	115.	109.	102.
435.	109.	127.	126.	124.	123.	120.	117.	110.	104.	98.
450.	94.	116.	119.	118.	117.	114.	111.	106.	100.	95.
465.	82.	107.	113.	112.	111.	108.	106.	101.	96.	91.
480.	71.	98.	108.	107.	105.	103.	101.	97.	93.	88.
495.	62.	90.	102.	101.	100.	98.	97.	93.	89.	85.
510.	55.	83.	97.	96.	95.	94.	92.	89.	86.	83.
525.	48.	76.	92.	91.	91.	89.	88.	85.	83.	80.
540.	42.	70.	87.	87.	86.	85.	84.	82.	80.	78.
555.	37.	64.	83.	82.	82.	81.	80.	79.	77.	75.
570.	33.	59.	79.	78.	78.	77.	77.	75.	74.	73.
585.	31.	54.	74.	74.	74.	74.	73.	73.	72.	71.
600.	32.	49.	71.	71.	70.	70.	70.	70.	69.	69.

Additionally, a number of evaluations were made in which this dry-out possibility was ignored and temperatures in the aqueous phase were allowed to exceed 100°C. This latter approach was initially viewed as probably being conservative because temperature has an important influence on silica solubility and thus on the quantity of rock that dissolves and subsequently precipitates.

MODEL

As stated in the previous section, the groundwater was assumed to always be in equilibrium with amorphous silica. The solubility of this polymorph of silica as a function of temperature is given by the following equation (Marshall, 1980):

$$\text{SOL} = \exp[-0.2729 - (2.5932 \times 10^3/T) + (5.3671 \times 10^5/T^2) - (8.4714 \times 10^7/T^3)] \quad (4)$$

where

SOL = amorphous silica solubility limit (mol/kg of water)

T = temperature (Kelvin).

A Fortran computer program was written to determine the temperature distribution, as a function of time and position, the corresponding amorphous silica solubility, the incremental quantity of silica dissolved or precipitated, and the cumulative change in porosity. The effects of water flow rate, initial rock porosity, power density, and time on the porosity change were evaluated. To allow the hydraulic system of the mountain to be simulated, the 600 m of rock along the vertical centerline of the repository was divided into the six stratigraphic units previously identified in Figure 1. It was assumed that the initial matrix porosity of each of the units was constant and uniformly distributed. The thickness, initial average matrix porosity, and identification for each of these units is given in Table 3 (Nimick, 1984).

The computation procedure that was used consisted of the following general steps:

Table 3. Definition and relevant properties for the six stratigraphic units considered.

<u>Code</u>	<u>Name</u>	<u>Average matrix porosity</u>	<u>Approximate thickness (m)</u>
IA2	Tiva Canyon (welded)	0.11	53
IB	Paintbrush Tuff (non welded)	0.40	85
IIA	Topopah Spring (lithophysae-rich)	0.15	179
IIB	Topopah Spring (lithophysae-poor)	0.12	107
IIIA	Topopah Spring (vitrophyre)	0.04	17
IIIB/ IVA	"Calico Hills"	0.33	159

1. Each of the six stratigraphic zones was divided into blocks, 1 square meter horizontally by a thickness that equaled the distance the water travels in the time step chosen. This distance is given by the following equation:

$$\delta = \frac{(\Delta t)(FR)}{(\phi)(s)} \quad (5)$$

where

- δ = thickness,
- Δt = time step,
- FR = water flux (either percolation rate for matrix flow or fracture flow rate for fracture flow),
- ϕ = matrix or fracture porosity, and
- s = fraction of the pores or fractures that is saturated.

The block (grid) structure is shown schematically in Figure 4. This figure graphically shows how matrix porosity differences between each stratigraphic unit affect the size of the block. It should be noted that in the first evaluations made, the initial porosity and fraction of the matrix which was saturated (and thus the block size) were each assumed to be a single value for all six stratigraphic units. This procedure was followed to allow the important effects on cumulative porosity change to be clearly identified.

2. A time increment was selected for the water flow rate being considered such that the block size would be a maximum of approximately 1-2 meters (except for the low porosity IIIA unit). The number of blocks in each stratigraphic unit was determined by dividing the thickness of each block into the approximate thickness of each unit as given in Table 3. The time was then stepped from zero to, in general, 10,000 years with the selected increment. At each time interval, steps 3 to 5 below were followed.
3. The temperature for each block was computed at the corresponding depth along with the amorphous silica solubility based on that temperature.

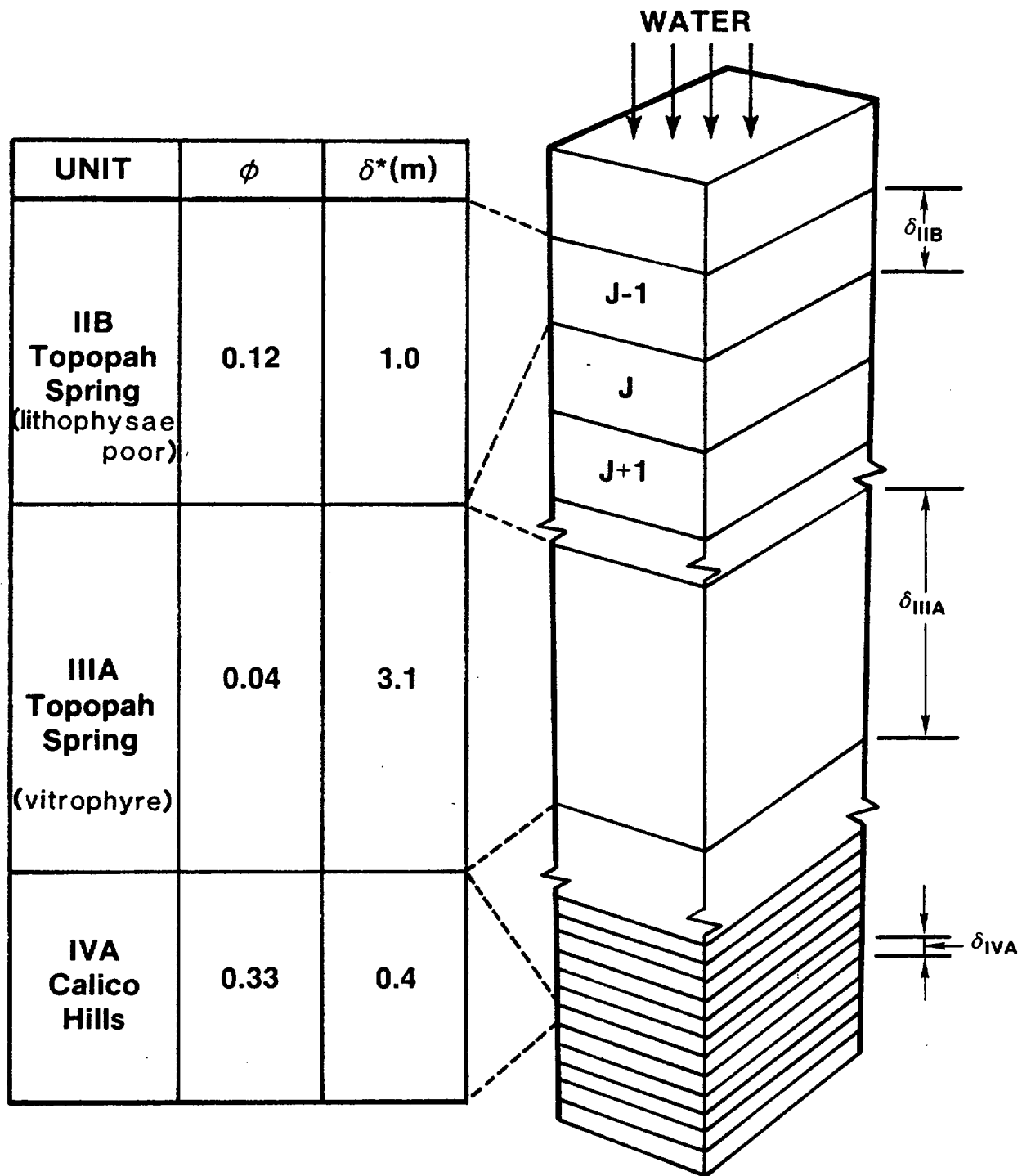


Figure 4. Schematic diagram of the block or grid structure used in the mineral dissolution and precipitation model.

4. The difference in silica concentration due to precipitation or dissolution was calculated for each block by subtracting the silica solubility for the conditions existing in the current block from the silica solubility the same packet of water had during the previous time step (see Figure 4). Mathematically, the change in the quantity of silica contained within the block j over the time interval $t_i - t_{i-1}$ is given by

$$\Delta q_{i,j} = (MW)(FR)(\Delta t_i)(SOL_{i-1,j-1} - SOL_{i,j})(\rho_w) \quad (6)$$

where

- $\Delta q_{i,j}$ = change in the quantity of silica with a given block
 Δt_i = $t_i - t_{i-1}$
 ρ_w = density of the groundwater
 MW = molecular weight of silica (60 g/mol)
 $SOL_{i,j}$ = amorphous silica solubility at time i in block j

The volume change of water due to the dissolution and precipitation of silica and temperature was neglected. Before the initial time step, the water in each block was assumed to be saturated with amorphous silica at the temperature of the existing geothermal gradient.

5. If the quantity calculated with equation (6) was negative (dissolution), a density of 2.33 g/cc (cristobalite) was used to calculate the volumetric change; if the quantity was positive (precipitation), a density of 2.2 g/cc (amorphous silica) was used. The final result is a cumulative change in porosity as a function of time and position calculated with the following equation:

$$\Delta \phi_j = \sum_{i=1}^{N_t} \frac{\Delta q_{i,j}}{(\rho_k)(\delta)(1 \text{ m}^2)} \quad (7)$$

where

- $\Delta\phi_j$ = cumulative porosity change for block j,
 N_t = total time/ Δt , and
 ρ_k = silica density (as described above).

6. For the evaluations in which the water was allowed to vaporize and the rock to dry out, the steps below were followed:

- a) Whenever the temperature of a block exceeded 100°C, the concentration of dissolved silica within that block was maintained at zero. Although the actual boiling temperature of water at the approximate repository elevation is 96°C, the higher temperature was used for convenience, and the potential effects of vapor pressure lowering and pore pressurization were ignored. This procedure resulted in an instantaneous precipitation of all the silica dissolved in the groundwater in the region heated to more than 100°C by the emplacement of waste; then, as time proceeded and the temperature in new regions exceeded 100°C, the silica contained in the groundwater flowing into these regions was deposited. As the 100°C isotherm receded, groundwater was allowed to flow in and re-equilibrate with the previously dry rock. Thus, the boundary of this dry zone was dynamic.
- b) When the water was vaporized, it was assumed to be removed from the system. Physically, this phenomena could occur if the emplacement boreholes are permeable to vapor. The groundwater percolating downward was assumed to be unable to penetrate the 100°C isotherm, but rather to flow instantaneously around the dry zone. With the high suction heads that exist in the rock (Peters and Gauthier, 1984), this latter assumption appears reasonable and is conservative; that is, this leads to an upper bound on silica-saturated water entering the region below the repository.

7. The temperature and cumulative porosity change results shown in this report represent averages over 15-m intervals. This procedure was used to ensure that all of the often rapidly changing, calculated quantities were included in the observed results.

RESULTS FOR CONSTANT POROSITY

The effect of a number of parameters on the cumulative change in porosity was first calculated assuming that only matrix flow occurs and that a single initial matrix porosity exists throughout the entire unsaturated zone being studied. This procedure is necessary to allow the important factors affecting the cumulative porosity change to be clearly identified and presented before the more complicated cases using actual stratigraphic data are discussed. The water flux through the matrix will be referred to as the percolation rate throughout the remainder of this paper. The effects of the individual parameters on the porosity change are discussed separately below. The case with a 57-kW/acre (14 W/m^2) spent fuel gross thermal loading, 0.5 mm/yr water percolation rate, 100-percent pore saturation, no water vaporization, and 12-percent matrix porosity was considered to be the base case with which most comparisons will be made. Again, these conditions are conservatively representative of those currently anticipated for Yucca Mountain.

Effect of Time

The effect of time on the cumulative porosity change for the base case conditions is shown in Figure 5. For reference, the data contained in this plot are listed in Table 4. All of the evaluations in which water percolation rate, matrix porosity, and thermal conditions were varied (at constant porosity) produced similar profiles. The most obvious result of these calculations is the expected direct correlation with the temperature profiles shown in Figure 2. As the water heats up, more rock dissolves, and as it cools, precipitation occurs. The maximum dissolution occurs at the point of highest temperature (the repository horizon) and decreases with increasing time (see Figure 6). The two following results are particularly worth noting:

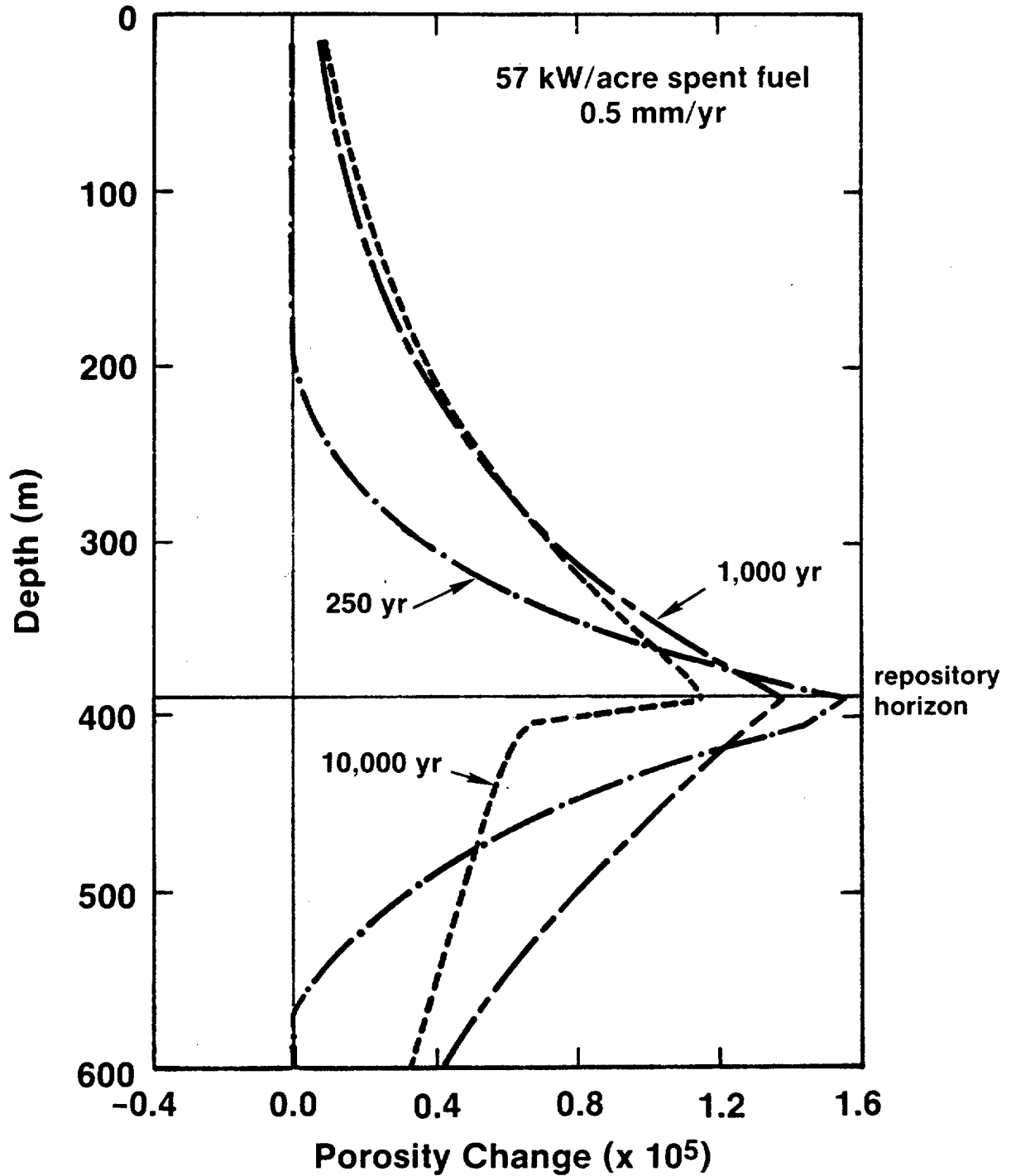


Figure 5. Cumulative matrix porosity change as a function of depth and time for a 57 kW/acre spent fuel repository contained in tuff with a single initial matrix porosity of 0.12, a constant percolation rate of 0.5 mm/yr, and no vaporization.

Table 4. Cumulative porosity change as a function of time and position for a hypothetical repository at Yucca Mountain (calculated at time from 250 to 10,000 years after emplacement) for the following conditions:

Waste type=spent fuel
 Water flux=0.5 mm/yr
 Time increment=62.5 years
 Matrix porosity=0.12

Areal power density=57 kW/acre
 Percent matrix saturation=100%
 Total number of blocks=2304

Cumulative Porosity Change (units of 1.E-05)

Depth (m)	250	500	1000	1500	2000	3000	4000	6000	8000	10000
15.	0.0	0.0	0.1	0.1	0.1	0.1	0.1	0.2	0.2	0.2
30.	0.0	0.0	0.1	0.1	0.1	0.1	0.1	0.1	0.1	0.1
45.	0.0	0.0	0.1	0.1	0.1	0.1	0.1	0.1	0.1	0.1
60.	0.0	0.0	0.1	0.1	0.1	0.1	0.1	0.1	0.1	0.1
75.	0.0	0.0	0.1	0.1	0.1	0.1	0.1	0.1	0.1	0.1
90.	0.0	0.0	0.1	0.1	0.2	0.2	0.2	0.2	0.2	0.2
105.	0.0	0.0	0.2	0.2	0.2	0.2	0.2	0.2	0.2	0.2
120.	0.0	0.1	0.2	0.2	0.2	0.2	0.2	0.2	0.2	0.2
135.	0.0	0.1	0.2	0.2	0.2	0.2	0.2	0.2	0.2	0.2
150.	0.0	0.1	0.2	0.2	0.2	0.3	0.3	0.3	0.3	0.3
165.	0.0	0.1	0.3	0.3	0.3	0.3	0.3	0.3	0.3	0.3
180.	0.0	0.2	0.3	0.3	0.3	0.3	0.3	0.3	0.3	0.3
195.	0.0	0.2	0.3	0.3	0.3	0.4	0.4	0.4	0.4	0.4
210.	0.0	0.2	0.4	0.4	0.4	0.4	0.4	0.4	0.4	0.4
225.	0.1	0.3	0.4	0.4	0.4	0.4	0.4	0.4	0.5	0.5
240.	0.1	0.4	0.5	0.5	0.5	0.5	0.5	0.5	0.5	0.5
255.	0.1	0.4	0.5	0.5	0.5	0.5	0.5	0.5	0.5	0.5
270.	0.2	0.5	0.6	0.6	0.6	0.6	0.6	0.6	0.6	0.6
285.	0.3	0.6	0.7	0.7	0.7	0.7	0.7	0.7	0.7	0.7
300.	0.4	0.7	0.7	0.7	0.7	0.7	0.7	0.7	0.7	0.7
315.	0.5	0.8	0.8	0.8	0.8	0.8	0.8	0.8	0.8	0.8
330.	0.6	0.9	0.9	0.9	0.9	0.9	0.9	0.9	0.9	0.9
345.	0.8	1.0	1.0	1.0	1.0	1.0	1.0	1.0	1.0	1.0
360.	1.0	1.2	1.1	1.1	1.1	1.1	1.1	1.1	1.1	1.0
375.	1.2	1.4	1.3	1.2	1.2	1.2	1.2	1.2	1.2	1.1
390.	1.6	1.6	1.4	1.4	1.4	1.3	1.3	1.3	1.2	1.2
405.	1.4	1.5	1.3	1.3	1.2	1.1	1.1	0.9	0.8	0.7
420.	1.2	1.3	1.2	1.2	1.1	1.1	1.0	0.9	0.7	0.6
435.	0.9	1.2	1.1	1.1	1.1	1.0	0.9	0.8	0.7	0.6
450.	0.8	1.1	1.0	1.0	1.0	0.9	0.9	0.8	0.7	0.6
465.	0.6	0.9	1.0	0.9	0.9	0.9	0.8	0.7	0.6	0.5
480.	0.5	0.8	0.9	0.9	0.8	0.8	0.7	0.7	0.6	0.5
495.	0.4	0.7	0.8	0.8	0.8	0.7	0.7	0.6	0.5	0.5
510.	0.3	0.6	0.8	0.7	0.7	0.7	0.6	0.6	0.5	0.5
525.	0.2	0.5	0.7	0.7	0.7	0.6	0.6	0.5	0.5	0.4
540.	0.1	0.5	0.6	0.6	0.6	0.6	0.5	0.5	0.5	0.4
555.	0.0	0.4	0.6	0.6	0.5	0.5	0.5	0.5	0.4	0.4
570.	0.0	0.3	0.5	0.5	0.5	0.5	0.5	0.4	0.4	0.4
585.	0.0	0.3	0.5	0.5	0.4	0.4	0.4	0.4	0.4	0.3
600.	0.0	0.2	0.4	0.4	0.4	0.4	0.4	0.4	0.3	0.3

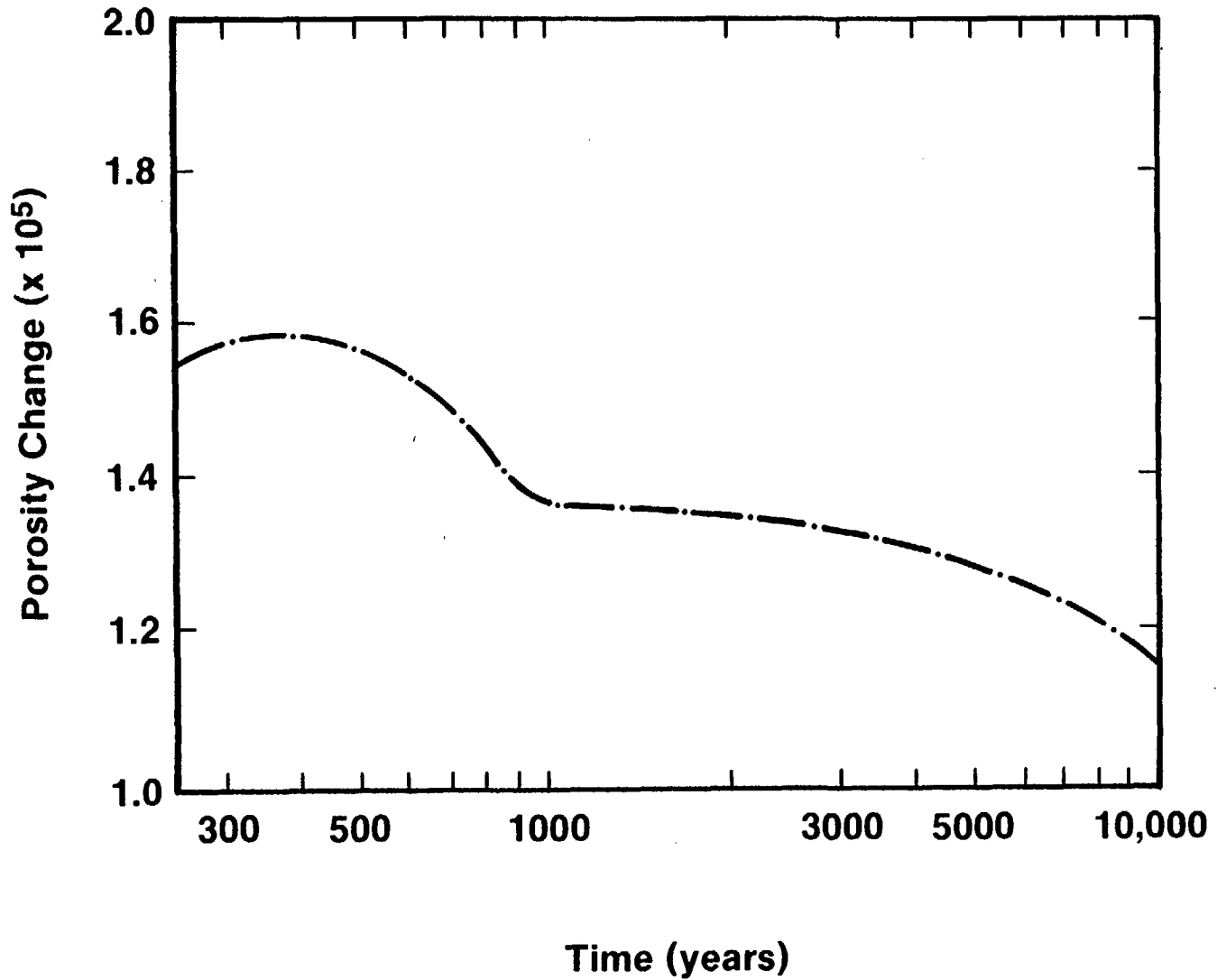


Figure 6. Cumulative matrix porosity change as a function of time at the depth of the repository for a 57 kW/acre loading in tuff with a single initial matrix porosity of 0.12, a constant percolation rate of 0.5 mm/yr, and no water vaporization.

1. The cumulative porosity changes are extremely small. The maximum increase occurred at 250-500 years and for these conditions (from Figure 5) was only 0.000016. Thus, if the initial porosity was 12 percent, then the maximum final porosity would be only 12.0016 percent, a relative variation ($\Delta\phi/\phi$) of approximately 0.02 percent. This compares with a relative variation in naturally occurring matrix porosity of 30 percent (Nimick, 1984). It is important to keep in mind while considering the different effects on cumulative porosity changes that all of the relative changes were calculated to be of this extremely low order of magnitude.
2. Net porosity decreases did not occur. During the 10,000-year period studied, the formation down to 600 m experienced a large enough overall gain in thermal energy to prevent any cumulative precipitation. With the essentially stagnant flow resulting from the expected low water flux, even if time were advanced farther, the porosity-change curves would continue to flatten (but never reach zero); the final porosity increase above 600 m would be balanced by an overall decrease in porosity somewhere below the water table.

Effect of Initial Matrix Porosity

The effect of assuming a different initial matrix porosity (assumed to be constant throughout the 600 meters for each case) is shown in Figure 7. The base case initial porosity of 12 percent (representative of the densely welded Topopah Spring) was changed to 33 percent (observed for the Calico Hills unit). An increase in the initial matrix porosity has the effect of decreasing the water velocity and, therefore, the quantity of rock that a given amount of water is exposed to during any time period. Since the concentration of silica in the water at a given time and depth is constant (the temperature profiles are independent of the initial porosity), the quantity of silica that dissolves or precipitates in a given block of rock must therefore increase as the initial matrix porosity is increased. The conclusion is confirmed in Figure 7, where the magnitude of the porosity change is shown to be directly proportional to the difference in initial matrix porosity. This same relationship holds at the longer time periods evaluated.

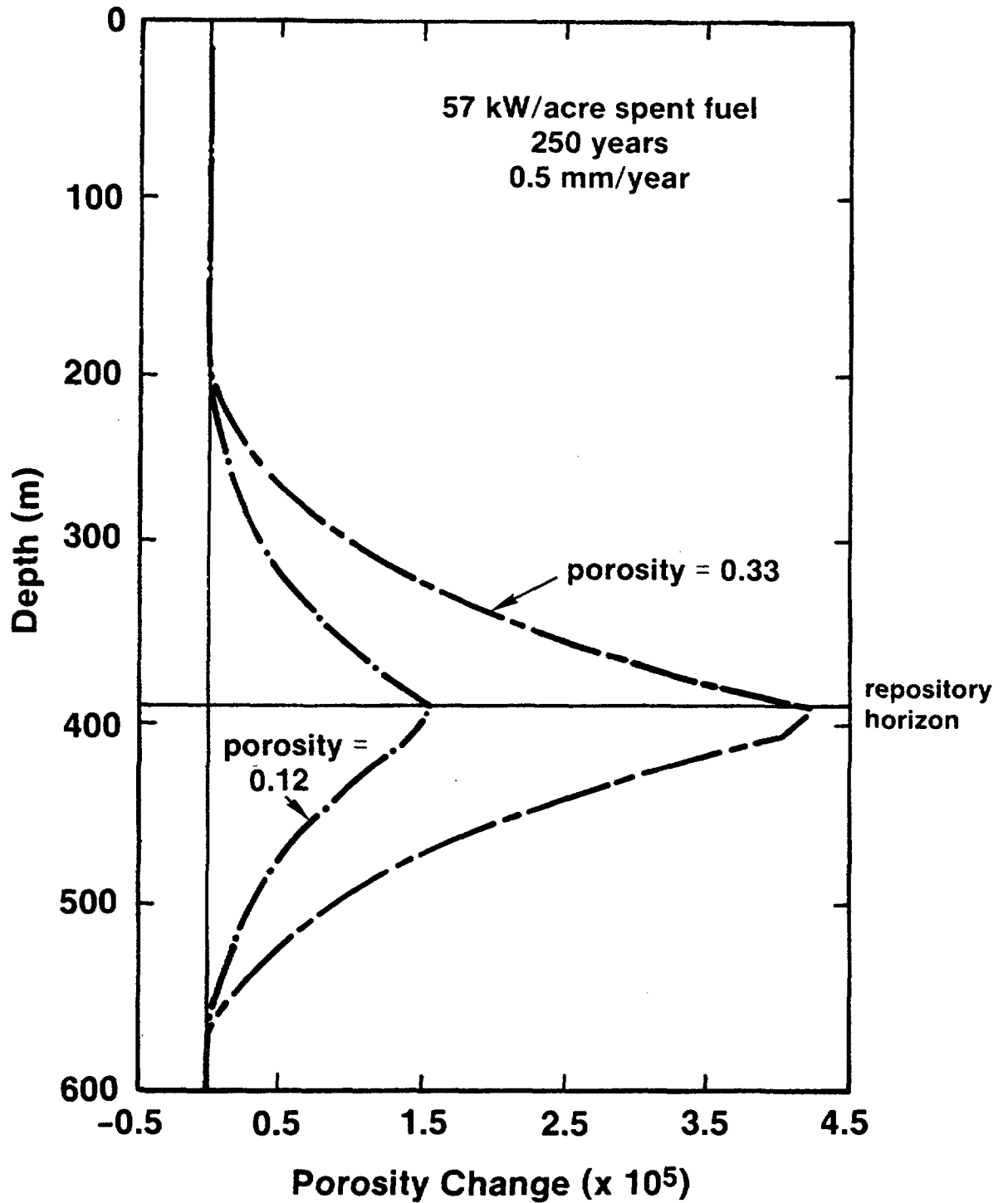


Figure 7. Cumulative matrix porosity change as a function of depth and initial matrix porosity at 250 years and a percolation rate of 0.5 mm/yr for a 57 kW/acre spent fuel repository. The 0.12 porosity is representative of the densely welded Topopah Spring Member and the 0.33 of the underlying "Calico Hills."

Effect of Percolation Rate and Pore Saturation

The effect of percolation rate and pore saturation on cumulative porosity change is shown in Figure 8. The percolation rates and saturation values used in this comparison are consistent with the pressure and saturation measurements made on core from Yucca Mountain (Peters and Gauthier, 1984).

As shown, the effect of percolation rate under these assumed conditions is limited. This lack of effect probably results because the quantity of solids transported between areas is dominated by temperature differences and not by the actual flow of water (since the concentration of dissolved solids and groundwater velocity are so small). As the percolation rate increases, a more significant transfer of water occurs between blocks, and the temperature-gradient effects become accentuated, as demonstrated by the dramatic decrease in the 1-mm/yr response curve immediately below the repository horizon.

A decrease in saturation has the same effect as reducing the initial matrix porosity (see equation 5). The "effective matrix porosity" for the calculation assuming 0.1 mm/yr, 50-percent saturation is therefore half that for the calculation assuming 0.1 mm/yr, 100-percent saturation. This difference, as explained in the preceding subsection, accounts for the observed change between the two curves for the lowest percolation rate.

Effect of Areal Power Density

The effect of higher temperature (due to increased power density) on the cumulative porosity increase is shown in Figure 9. The characteristics and relative differences of the responses shown in this figure are qualitatively similar when variations in time and percolation rates are considered. Higher rock temperatures simply increase the magnitude of the porosity changes.

Effect of Water Vaporization

The effect of allowing water to vaporize and therefore the rock to dry out is shown in Figures 10, 11, and 12. Figure 10 shows this effect as a function of time for the lower, 57-kW/acre (14 W/m^2), loading. The deep spikes shown in these figures originate from the immediate precipitation of the silica that was dissolved in the groundwater before the emplacement of waste. It should

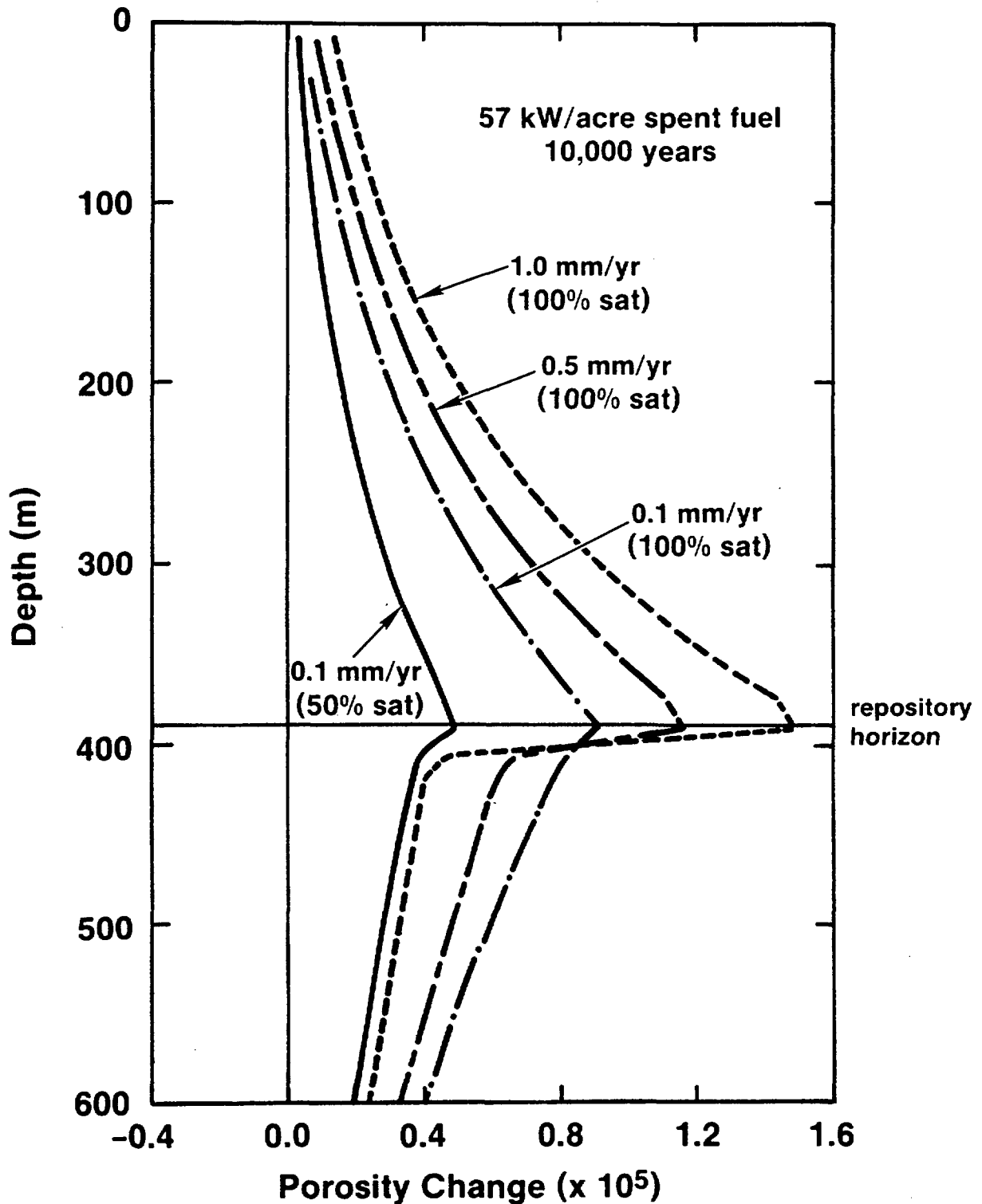


Figure 8. Cumulative matrix porosity change as a function of depth, percolation rate, and saturation for a 57 kW/acre spent fuel repository with a single initial matrix porosity of 0.12 at 250 years following emplacement and no water vaporization.

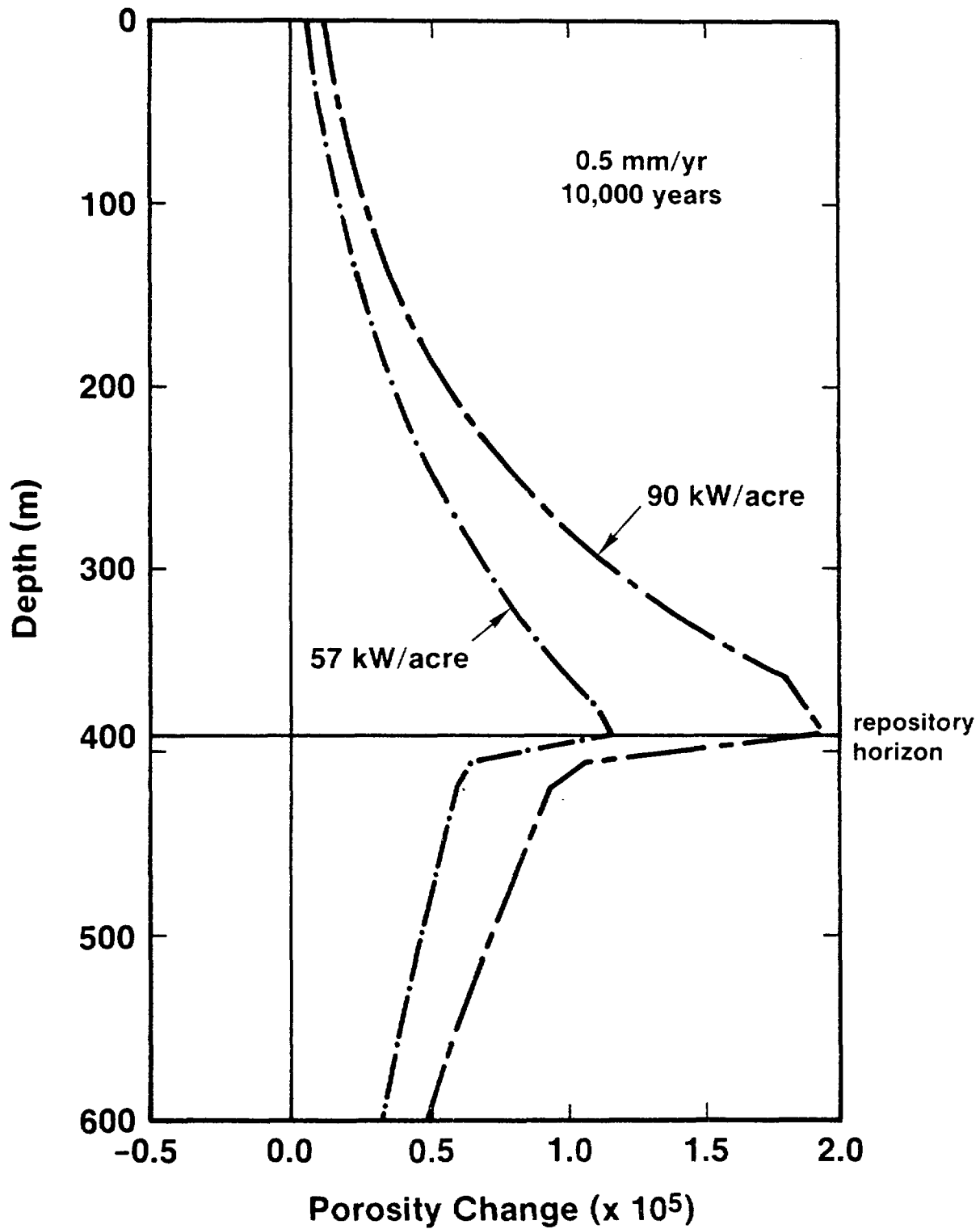


Figure 9. Cumulative matrix porosity change as a function of depth for the two area power densities considered and a single initial matrix porosity of 0.12, a percolation rate of 0.5 mm/yr, no water vaporization, and at 10,000 years following emplacement.

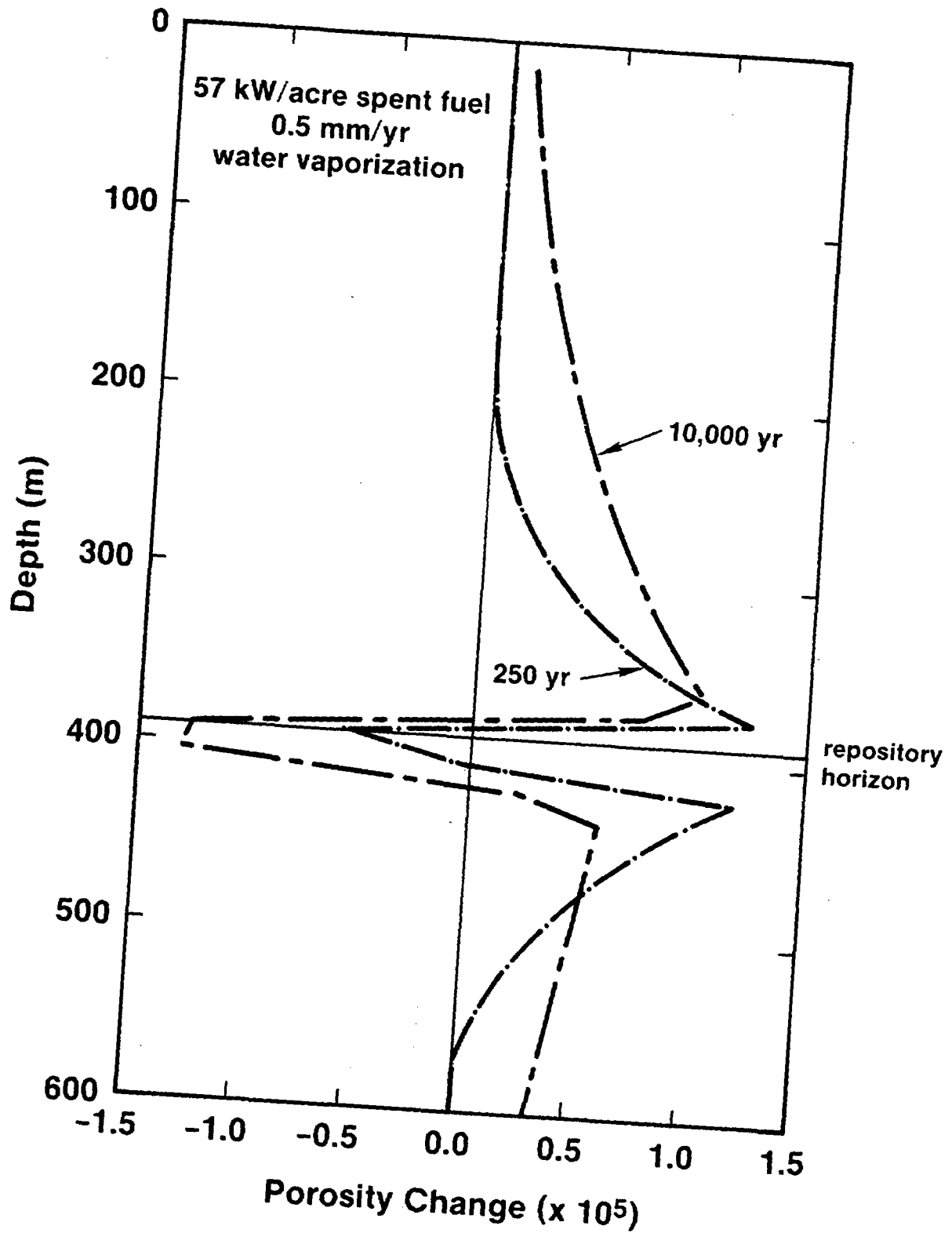


Figure 10. Cumulative matrix porosity change as a function of depth and time for a 57 kW/acre spent fuel repository with a single initial matrix porosity of 0.12, a constant percolation rate of 0.5 mm/yr, and water vaporization for regions in which the temperature exceeded 100°C.

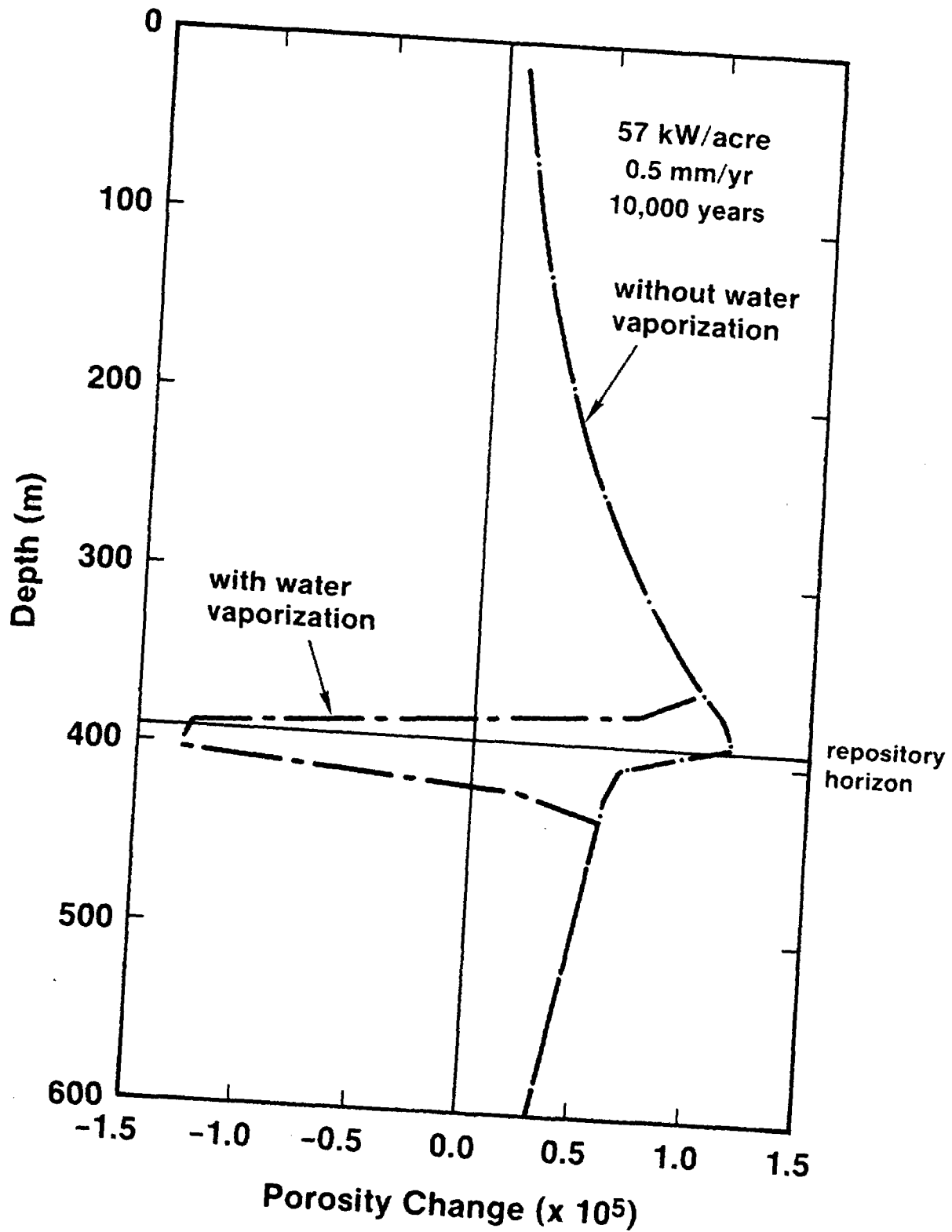


Figure 11. Cumulative matrix porosity change as a function of depth with and without water vaporization for a 57 kW/acre spent fuel repository with a single initial matrix porosity of 0.12, and a constant percolation rate of 0.5 mm/yr.

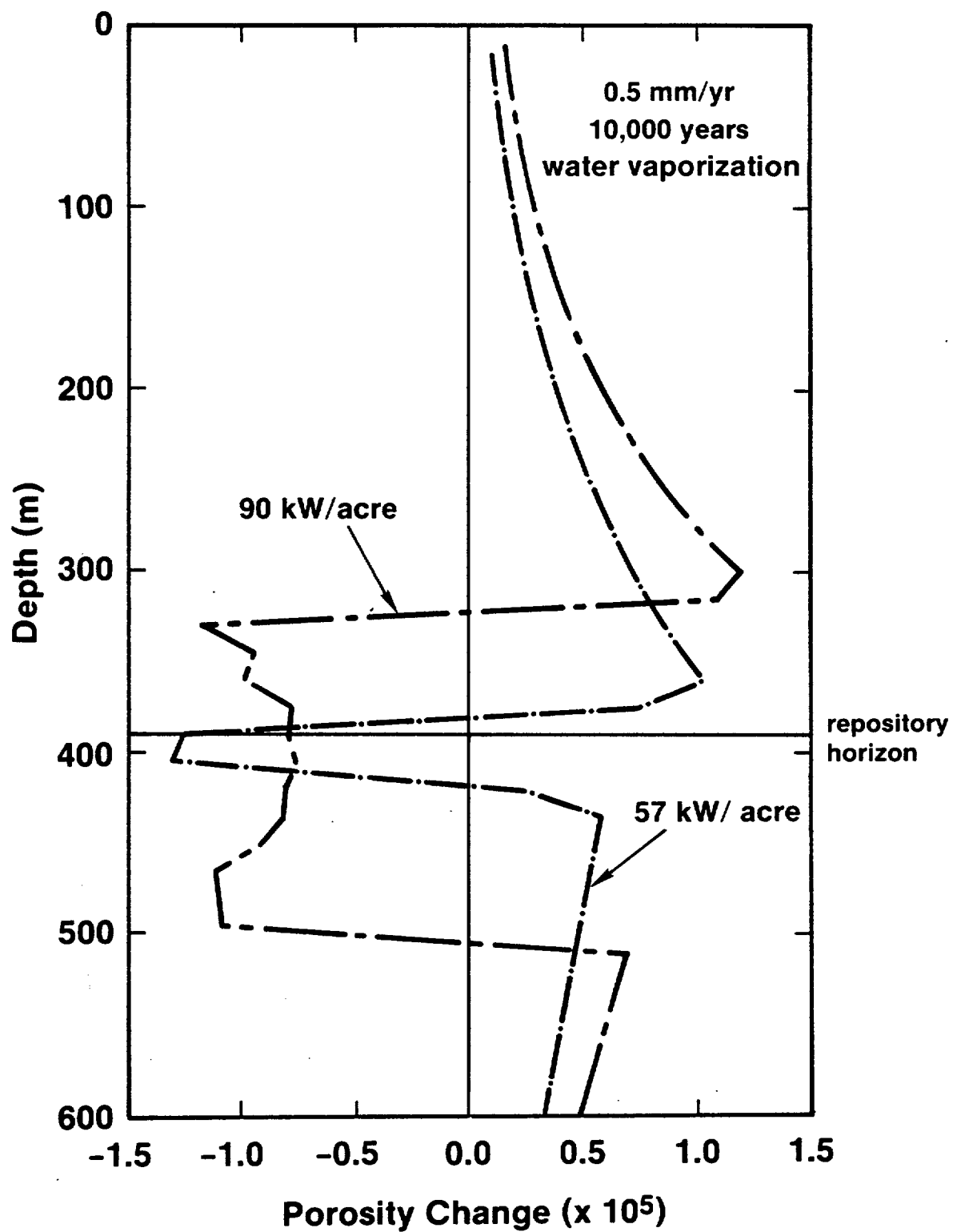


Figure 12. Cumulative matrix porosity change as a function of depth for the two areal power densities considered and a single initial matrix porosity of 0.12, a percolation rate of 0.5 mm/yr, water vaporization, and at 10,000 years following emplacement.

be remembered that at this loading the temperature exceeds 100°C only in regions immediately around the repository level and for times less than 1000 years. The deepening of the spikes is caused by the same net precipitation processes that reduced the maximum value of the porosity-change curves shown previously in Figure 5. As shown in Figure 11, the porosity-change responses are identical to those in which vaporization was not allowed in the regions where the temperature did not exceed 100°C. Figure 12 shows the long-term effect of increasing the loading to 90 kW/acre (22 W/m²). At this increased loading, the region experiencing temperatures above 100°C initially grows with time. This causes more material to precipitate in the affected region, and thus the width of the spike increases.

RESULTS FOR VARIABLE MATRIX POROSITY

The initial porosity of the matrix was shown in the previous section to have an important effect on the relative magnitude of the changes produced in the porosity. For this reason, the matrix and fracture porosity within each stratigraphic unit must be included when predicting cumulative porosity changes that could actually occur beneath Yucca Mountain. Again, the primary concern with the dissolution and precipitation of host-rock minerals is that a significant decrease in permeability may be produced. As shown above, regions in which cumulative porosity changes were negative only occurred when water was allowed to vaporize.

In this section, the effects of time, percolation rate, and areal power density on cumulative porosity change are given for the conditions of expected matrix flow, constant initial matrix porosity throughout each major stratigraphic units, and water vaporization if the temperature exceeds 100°C. These results will be used in the important subsequent analysis of potential matrix permeability changes. This type of analysis also forms the basis for evaluating fracture flow.

The effect of time on the change in porosity for the two areal power densities being considered is shown in Figures 13 and 14. It is important to keep in mind that higher initial matrix porosity values decrease the quantity of rock with which a given volume of water can interact (by decreasing flow speed) and therefore increase the magnitude of the cumulative porosity change

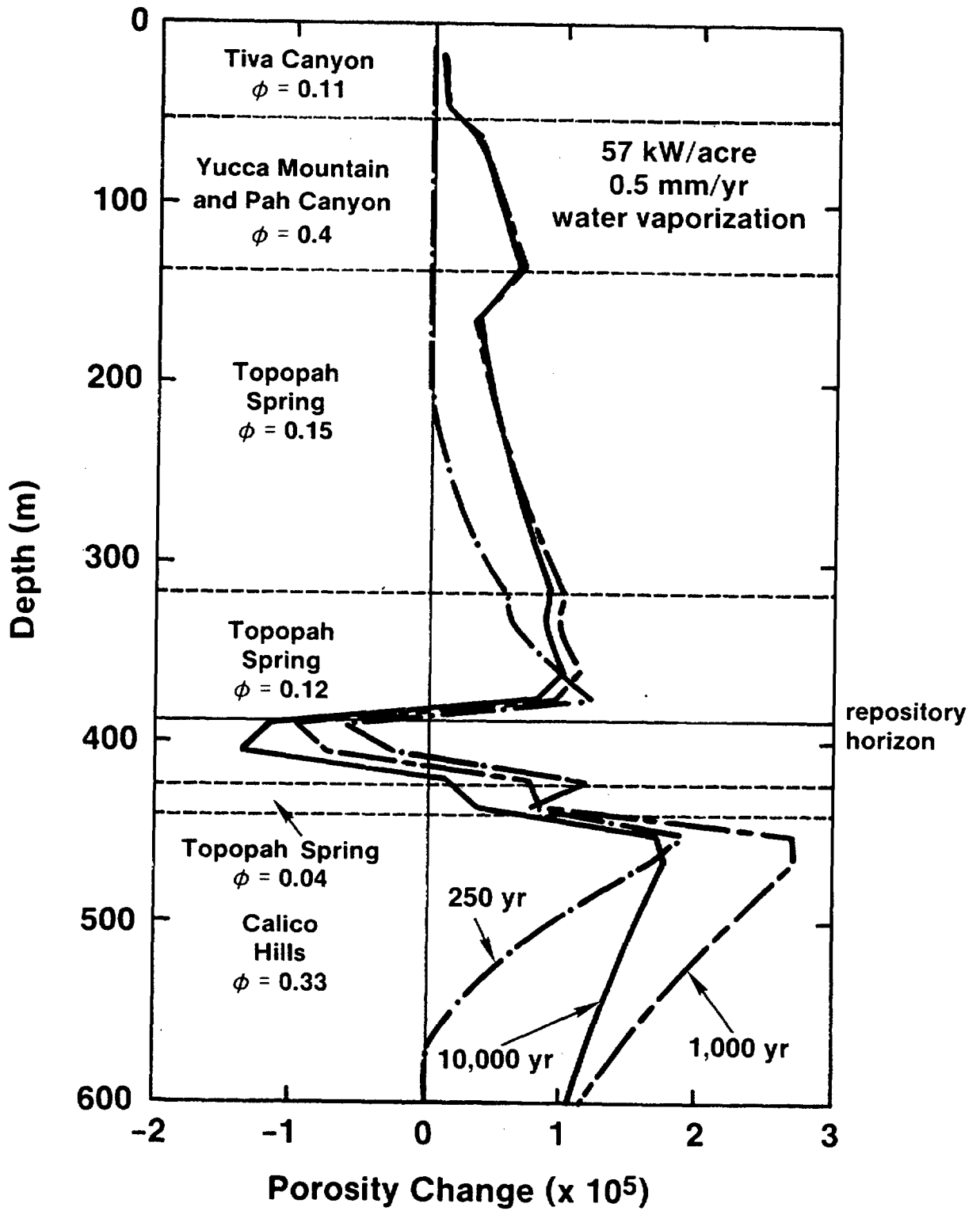


Figure 13. Cumulative matrix porosity change as a function of depth and time for a 57 kW/acre spent fuel repository using the initial matrix porosity of each strati-graphic unit, a constant percolation rate of 0.5 mm/yr, and water vaporization.

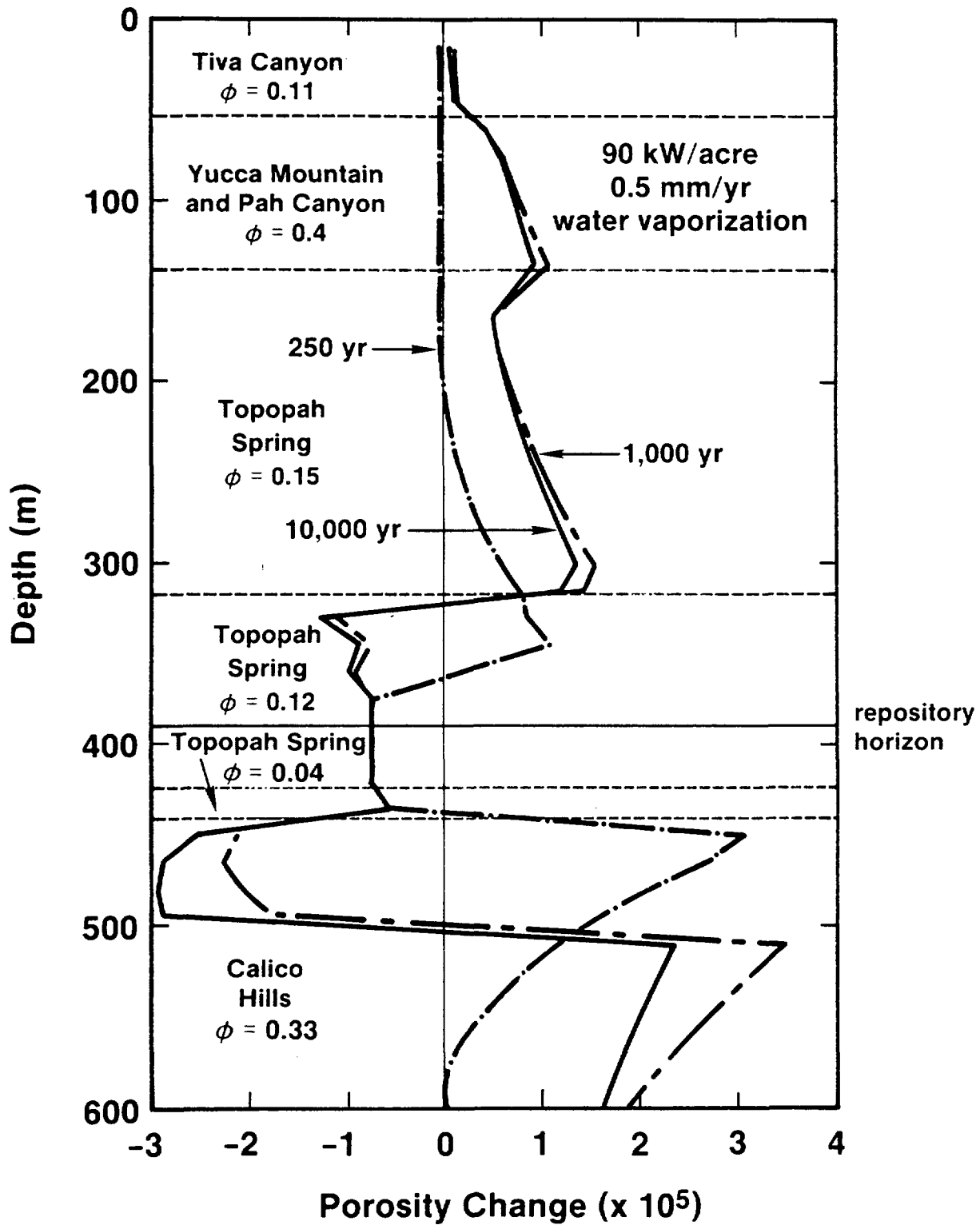


Figure 14. Cumulative matrix porosity change as a function of depth and time for a 90 kW/acre spent fuel repository using the initial matrix porosity of each stratigraphic unit, a constant percolation rate of 0.5 mm/yr, and water vaporization.

produced (refer back to Figure 7). The deviation in the general shapes of these responses from those shown in the previous section is due to this significant effect. To demonstrate this conclusion, compare the 10,000-year curve shown in Figure 13 to the 10,000-year curve shown in Figure 10. The increases in cumulative porosity change shown in Figure 13 over those in Figure 10 for the nonwelded Paintbrush tuffs and the "Calico Hills" regions occur because the initial matrix porosity has been changed from 0.12 to 0.4 and 0.12 to 0.33, respectively. The decrease through the vitrophyre region (IIIA) results from an initial matrix-porosity change from 0.12 to 0.04.

The effect of percolation rate on the cumulative porosity change for matrix flow conditions is shown in Figure 15. As in Figure 8, for the same initial porosity throughout all rock units, a major portion of the difference between these two curves occurs because the matrix is not saturated when the rate is 0.1 mm/yr (effectively halves the matrix porosity for every unit). Thus, the impact of percolation rate under the currently expected conditions of matrix flow is not significant.

RESULTS FOR PERMEABILITY CHANGES

The study of water flow through the Topopah Spring Member recently conducted by Peters and Gauthier (1984) resulted in three conclusions important to this evaluation:

1. An average water percolation rate of 0.1 mm/yr or less through the Topopah Spring is consistent with pressure and saturation measurements.
2. At this percolation rate, saturation is less than 1.0, and the suction heads are sufficiently high that water movement will take place only in the pores.
3. The saturated hydraulic conductivity of the Topopah Spring matrix is less than $1.5E-10$ to $3.9E-9$ cm/sec, which is sufficient to support percolation rates of 0.05 to 1.2 mm/yr. At water flow rates greater than the saturated conductivity of the matrix, fracture flow is expected to occur.

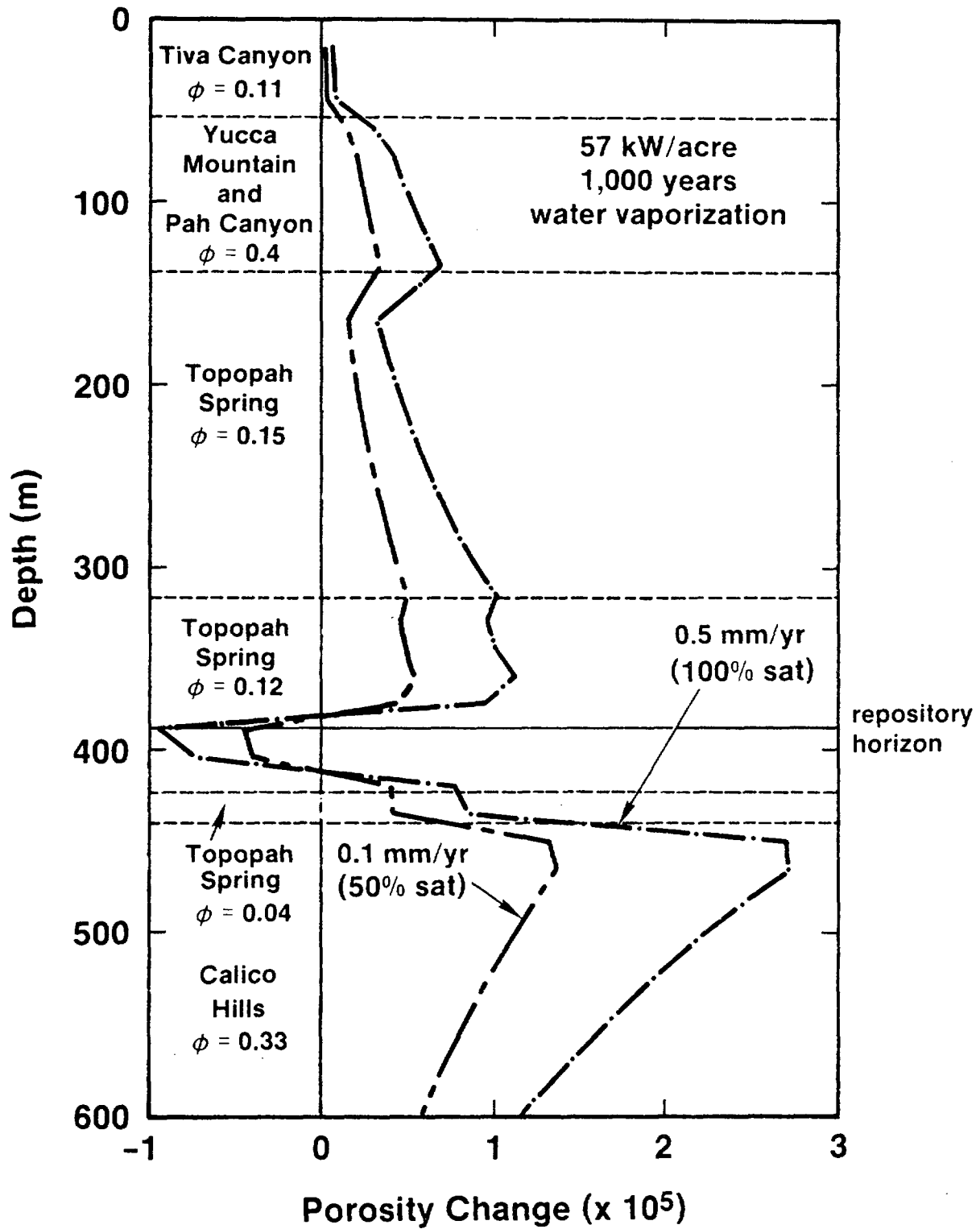


Figure 15. Cumulative matrix porosity change as a function of depth and percolation rate for a 57 kW/acre spent fuel repository using the initial matrix porosity of each stratigraphic unit, and water vaporization.

Matrix Flow

Since the projections made by Peters and Gauthier (1984) showed that matrix flow should dominate the hydraulic system for all of the unsaturated units beneath Yucca Mountain, most dissolution and precipitation reactions should occur within the pores. The results presented in the previous section show that the largest relative effect ($\Delta\phi/\phi$) of host-rock mineral dissolution and precipitation occurs within the Topopah Spring unit (see Figure 14). This result is because the greatest temperature gradient occurs in the Topopah Spring unit. Using the largest observed relative increase, the initial 15-percent matrix porosity would increase to 15.0016 percent. The largest observed cumulative decrease would change the initial 12 percent matrix porosity to 11.9988 percent. These small calculated effects would be undetectable among the naturally occurring variations.

Fracture Flow

The effect of host-rock reactions on the permeability of the fractures must also be addressed in order to estimate the consequences of a potential climatic change and a resultant water flow rate greater than 0.5 mm/yr. Fracture flow was only studied in the Topopah Spring units because, as shown in the previous analyses, these are the only units in which a net precipitation of silica occurred.

For laminar flow between parallel plates (a common approximation for fracture flow), aperture (e) and fracture permeability (K) may be related by (Snow, 1968)

$$K = \frac{e^2}{12} \quad (8)$$

Thus, the change in permeability due to a change in aperture may be represented by

$$\Delta K = K_i - K_f = \frac{e_i^2 - e_f^2}{12} \quad (9)$$

where subscript i refers to the initial state and subscript f to the final state. The final aperture may be calculated from

$$e_f = e_i - \frac{V}{NA} \quad (10)$$

where

- V = volume of material precipitated (or dissolved) per unit length,
- N = number of fractures per unit length, and
- A = area of the fracture surface.

As expected, the change in permeability is affected by initial fracture aperture, the fracture density, and the volume of material dissolved or precipitated. Data given by Scott et al. (1983) give a range of fracture densities of approximately 16 to 32 fractures per meter in densely welded tuffs and about 7 fractures per meter in the vitrophyre of the Topopah Spring. Apertures of these fractures have not been measured, but the use of data given by Klavetter (1984) provides an estimate of 3 to 38 μm for equivalent hydraulic apertures of the fractures in the densely welded Topopah Spring. It is assumed here that hydraulic apertures will range from 5 to 50 μm . Since equivalent hydraulic apertures are smaller than actual geometric apertures, the porosity change described below will have a larger relative effect using this assumption.

The permeability for rock containing a set of parallel fractures may be calculated from (Snow, 1968):

$$K_i = \frac{Ne^3}{12} \quad (11)$$

Assuming that there are an average of 25 fractures per meter in the densely welded Topopah Spring, each with an average aperture of 30 μm , the hydraulic

conductivity due to fractures would be about 18,000 mm/yr.* In the vitrophyre, with seven fractures per meter and the same aperture, hydraulic conductivity would be about 5,000 mm/yr.

Since fluctuations in the flow rate great enough to exceed the conductivity of the fractures are unlikely, the fractures, as they currently exist, should be able to accommodate (i.e., transmit) all water flow above that which penetrates the matrix. This study examined the possibility that at some reasonable upper bound on the water flux (here assumed to be 4.5 mm/yr, or 4 mm/yr in the fractures), host-rock dissolution and precipitation might decrease the fracture conductivity to the point where some amount of the water inflow would be diverted to flow in an approximately horizontal direction.

Figure 16 shows the porosity changes for the matrix flow as well as for fracture flow with two different fracture porosities. The total porosity change after 250 years at a flow rate of 4.5 mm/yr would be the sum of changes in matrix and fracture porosity, or a volume fraction of about 0.000013. However, this may be misleading. Material precipitated in fractures will decrease conductivity to a more significant extent than the same quantity of precipitate would decrease matrix conductivity.

The data used in Figure 16 also show that there is little difference in the porosity change for initial fracture porosities of 0.0001 and 0.001.** Thus, the larger relative change of porosity would occur for an initial fracture porosity of 0.0001. This porosity change is assumed to be distributed between 20 fractures per meter with an aperture of 5 μm , each a value within the range in these properties mentioned earlier. The bulk fracture conductivity of such a material (ignoring matrix conductivity) would be 66 mm/yr.

The maximum precipitation of material occurs when the water vaporizes, and this vaporization has the largest effect at the repository horizon (Figure 16).

*Equation 11 provides a permeability in units of length squared. In order to convert to hydraulic conductivity, with units of length per time, the following equivalence was used: $1 \text{ cm/sec} = 10^{-5} \text{ cm}^2$.

**These two values were selected for computational convenience, and are assumed to be representative of the expected minimum values of fracture porosity in the Topopah Spring Member.

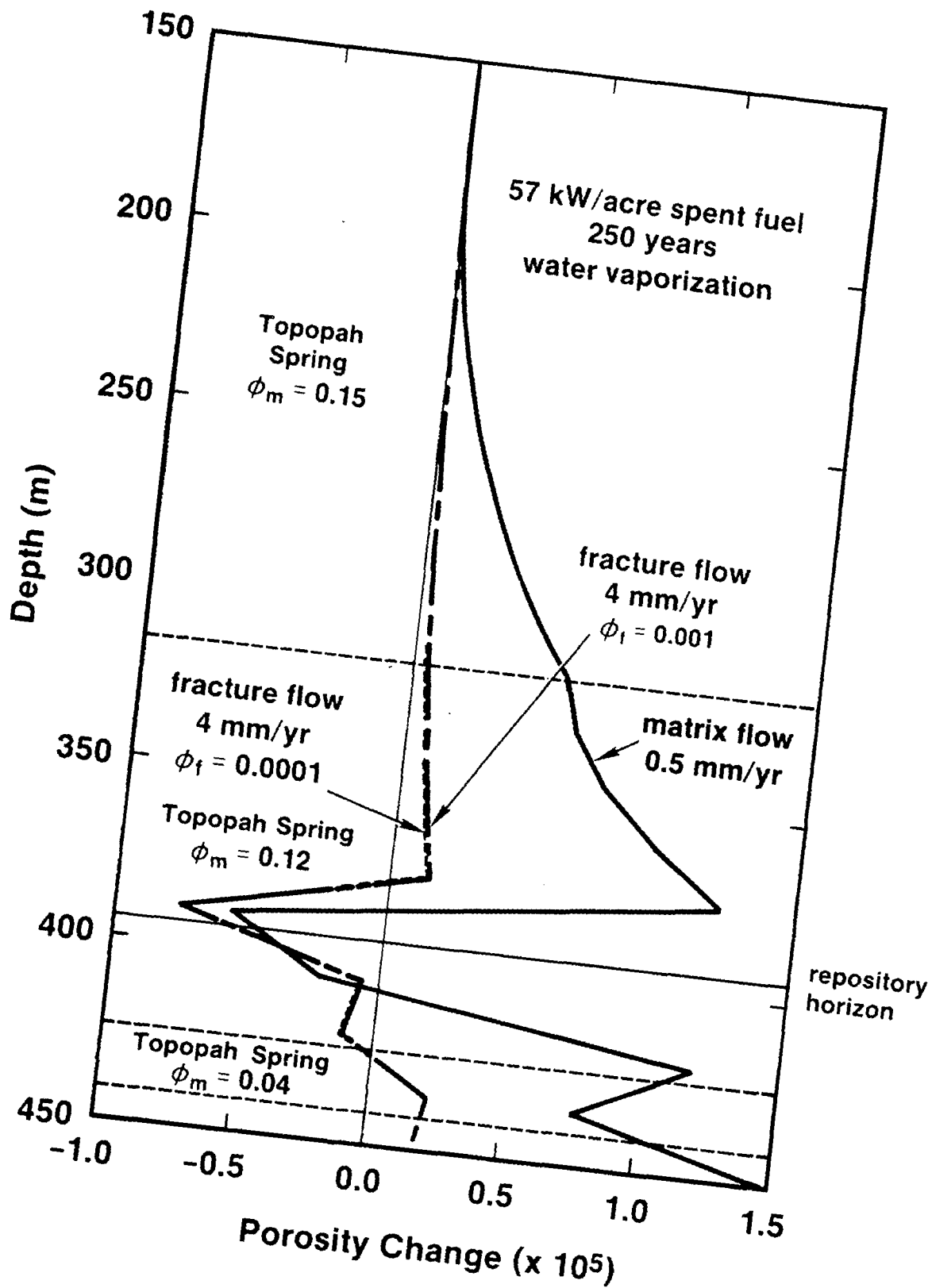


Figure 16. Comparison of the cumulative porosity changes in the matrix and the fractures of the Topopah Spring Member at 250 years after the emplacement of a 57 kW/acre spent fuel repository beneath Yucca Mountain.

The greatest net quantity of material precipitated will be the product of the largest net porosity change and the volume of the block, or $3.2\text{E-}05 \text{ m}^3$ for a 1-m thick block and a porosity change of 3.2×10^{-5} at a time of 1000 years. According to equation (10), the final fracture aperture would be 3.4 μm , which results in a calculated bulk hydraulic conductivity of 21 mm/yr, or a decrease of about 70 percent. However, with the assumed maximum fracture flux being 4 mm/yr, the difference between 66 mm/yr and 21 mm/yr will not change the ability of the fractures to transmit all of the available water.

Although dissolution can only increase an already large conductivity, it is instructive to examine the relative change. Maximum dissolution at 4 mm/yr is predicted to occur at a depth of 150 m (near the top of the densely welded Topopah Spring) at a time of 10,000 years, and is about $12.2\text{E-}05 \text{ m}^3$ for a 2.5-m-thick block. Assuming the same fracture distribution as given in the two preceding paragraphs, the final fracture aperture would be 7.4 μm , giving a final hydraulic conductivity of 216 mm/yr. Thus, the bulk fracture conductivity would increase by a factor of three. However, since even the initial fracture conductivity is greater than that necessary to transmit the anticipated water flux, this increase will not have a significant impact on flow patterns.

It should be kept in mind that these numbers are conservative. Even with climatic changes, water flow rates are likely to be even lower than 4 mm/yr, and fracture porosity is more likely to be closer to 0.001 than to 0.0001.

SUMMARY

This study was conducted to effectively bound the effect of thermally-induced dissolution and precipitation of the host rock on alterations of the hydrologic properties of the tuffs at Yucca Mountain. The important results of this study include the following:

1. In the tuff beneath Yucca Mountain, the dissolution and precipitation of minerals due to their interaction with heating and cooling groundwaters can be conservatively described by assuming that the groundwater is always in equilibrium with amorphous silica.

2. The results of coupling amorphous-silica-equilibrated groundwater flow with the thermal distribution produced by the emplacement of spent fuel shows several relevant features:
- a) The resultant cumulative porosity changes qualitatively correlate with the temperature profiles. Thus, as expected, in regions where water is being heated, the porosity increases; and in regions where water is cooling, the porosity decreases. Additionally, porosity changes for a 90-kW/acre (22 W/m^2) loading are higher than those for a 57-kW/acre (14 W/m^2) loading.
 - b) Only very small increases in cumulative porosity are predicted to occur. With expected percolation rates, the maximum increase for any of the conditions considered is a volume fraction of 0.000016. These changes are several orders of magnitude smaller than the observed natural variation in porosity.
 - c) Net cumulative porosity decreases do not occur in the calculations unless water is assumed to vaporize. Even with water vaporization, the porosity decrease is limited to approximately 0.000012.
 - d) Differences in water flow from 0.1 to 4 mm/yr have only a minimal affect on cumulative porosity change.
3. The important issue of whether or not host-rock dissolution and deposition could produce significant decreases in permeability was addressed for both regimes of potential water flow:
- a) If porous flow dominates (an assumption currently supported by field measurements and calculations for average percolation rates below 0.5 mm/yr), no observable increase or decrease in permeability should occur.

- b) If fracture flow dominates (for water fluxes in excess of 0.5 mm/yr), fracture permeabilities may show large changes, but even with these changes, the bulk permeability due to fractures is much greater than the amount of water which the fractures will be required to transmit. Thus, changes in fracture permeability will have no significant effect on the total hydrologic flow patterns through the mountain.

REFERENCES

- Bish, D. L., D. T. Vaniman, F. M. Byers Jr., and D. E. Broxton, 1982, "Summary of the Mineralogy-Petrology of Tuffs of Yucca Mountain and the Secondary-Phase Thermal Stability in Tuffs," Los Alamos National Laboratory Report LA-9321-MS, 47 pp.
- Broxton D., D. Vaniman, F. Caporuscio, B. Arney, and G. Heiken, 1982, "Detailed Petrographic Descriptions and Microprobe Data for Drill Holes USW-G2 and UE25b-1H, Yucca Mountain, Nevada," Los Alamos National Laboratory Report LA-9324-MS, 168 pp.
- Caporuscio, F., D. Vaniman, D. Bish, D. Broxton, B. Arney, G. Heiken, F. Byers, R. Gooley, and E. Semarge, 1982, "Petrologic Studies of Drill Cores USW-G2 and UE25b-1H, Yucca Mountain, Nevada," Los Alamos National Laboratory Report LA-9255-MS, 111 pp.
- Carroll, P. I., F. A. Caporuscio, and D. L. Bish, 1981, "Further Description of the Petrology of the Topopah Spring Member of the Paintbrush Tuff in Drill Holes UE25A-1 and USW-G1 and the Lithic-Rich Tuff in USW-G1, Yucca Mountain, Nevada," Los Alamos National Laboratory Report LA-9000-MS, 26 pp.
- Crerar, D. A., and G. M. Anderson, 1971, "Solubility and Solution Reactions of Quartz in Dilute Hydrothermal Solutions," *Chem. Geol.* 8:107-122.
- deBoer, R. B., P. J. C. Nagtegaal, and E. M. Duyvis, 1977, "Pressure Solution Experiments on Quartz Sand," *Geochem. Cosmochem. Acta.* 41:257-264.
- Fournier, R. O., 1977, "Chemical Geothermometers and Mixing Models for Geothermal Systems," *Geothermics* 5:41-50.
- Fournier, R. O., and J. J. Rowe, 1966, "Estimation of Underground Temperatures from the Silica Content of Water from Hot Springs and Wet-Steam Wells," *Amer. Jour. Sci.* 264:685-697.
- Heald, M. T., 1965, "Lithification of Sandstones in West Virginia," *W. Va. Geol. and Econ. Surv. Bull.* 30, 28 pp.
- Heald, M. T., and G. F. Baker, 1977, "Diagenesis of the Mt. Simon and Rose Run Sandstones in Western West Virginia and Southern Ohio," *Jour. Sed. Pet.* 47(1):66-77.
- Heiken, G. H., and M. L. Bevier, 1979, "Petrology of Tuff Units from the J-13 Drill Site, Jackass Flats, Nevada," Los Alamos National Laboratory Report LA-7563-MS, 55 pp.

- Holley, C., C. Grigsby, J. Tester, L. Blatz, and R. Charles, 1980, "Interaction of Water with Crystalline Basement Rock in Fractured Hot Dry Rock Geothermal Reservoirs: Tests and Laboratory Experiments," Proc. 3rd Int. Symp. on Water-Rock Interaction, Int. Assoc. Geochem. Cosmochem. and Alberta Res. Council, Edmonton, July 14-24, p. 161-162.
- Huang, W. H., and W. C. Kiang, 1972, "Laboratory Dissolution of Plagioclase Feldspars in Water and Organic Acids at Room Temperature," Amer. Miner. 57:1849-1859.
- Kennedy, G. E., 1950, "A Portion of the System Silica-Water," Econ. Geol. 45:629-653.
- Klavetter, E. A., 1984, "Fracture Hydrologic Property Data," Memo to Distribution, April 17, 1984.
- Marshall, W. L., 1980, "Amorphous Silica Solubilities-I. Behavior in Aqueous Sodium Nitrate Solutions: 25-300°C, 0-6 Molal," Geochem. Cosmochem. Acta. 44:907-913.
- Marshall, W. L., and J. M. Warakowski, 1980, "Amorphous Silica Solubilities-II. Effect of Aqueous Salt Solutions at 25°C," Geochem. Cosmochem. Acta. 44:915-924.
- Morey, G. W., R. O. Fournier, and J. J. Rowe, 1962, "The Solubility of Quartz in Water in the Temperature Interval from 25° to 300°C," Geochem. Cosmochem. Acta., 26:1029-1043.
- Morris, R. C., K. E. Proctor, and M. R. Koch, 1979, "Petrology and Diagenesis of Deep-Water Sandstones, Ouachita Mountains, Arkansas and Oklahoma," SEPM Spec. Pub. 26:263-279.
- Mosebach, R., 1957, "Thermodynamic Behavior of Quartz and Other Forms of Silica in Pure Water at Elevated Temperatures and Pressure with Conclusions on their Mechanism of Solution," Jour. Geol. 65(4):347-363.
- Nash, K. E., and C. E. Marshall, 1956, "The Surface Reactions of Silicate Minerals. Part II. Reactions of Feldspar Surfaces with Salt Solutions," Univ. of Missouri College of Agric., Agric. Expt. Sta. Res. Bull. 64, 36 pp.
- Nikitina, L. P., 1976, "The Behavior of Si, Fe, Al, and Ti in Hydrothermal Solution-Rock Interaction in Active Volcanoes," in Cadek, J. and Paces, T. (eds.) Proc. Int. Symp. on Water-Rock Interactions, Prague, September 9-17, 1974:196-201.

- Nimick, F. B., 1984, "Thermal-Mechanical Units at Yucca Mountain: Geometry and Material Properties," Sandia National Laboratories Report, SAND84-1076 (in preparation).
- Peters, R. R., and J. H. Gauthier, 1984, "Results of TOSPAC Hydrologic Calculations for Yucca Mountain," SNL Memo to F. W. Bingham, 6312, April 30, 1984.
- Pruess, K., and J. S. Y. Wang, 1983, "TOUGH-A Numerical Model for Nonisothermal Unsaturated Flow in Fractured Porous Media," Scientific Basis for Nuclear Waste Management, Vol. VI, Materials Research Society, (in press).
- Reardon, E. J., 1979, "Complexing of Silica by Iron(III) in Natural Waters," Chem. Geol. 25:339-345.
- Rimstidt, J. D., and H. L. Barnes, 1980, "The Kinetics of Silica-Water Reactions," Geochem. Cosmochem. Acta. 44:1683-1699.
- Scott, R. B., et al., 1983, "Geologic Character of Tuffs in the Unsaturated Zone at Yucca Mountain, Southern Nevada," in Mercer, J. (ed.) Role of the Unsaturated Zone in Radioactive and Hazardous Waste Disposal, Arbor Science, Ann Arbor, Michigan, pp. 289-335.
- Siever, R., 1962, "Silica Solubility, 0°-200°C, and the Diagenesis of Siliceous Sediments," Jour. Geol. 70(2):127-150.
- Snow, D. T., 1968, "Rock Fracture Spacings, Openings and Porosities," Jour. Soil Mech. and Found. Div., Proc. ASCE, 94:73-91.
- Sosman, R. B., 1965, "The Phases of Silica," Rutgers Univ. Press (New Brunswick, NJ), 387 pp.
- Svalstad, D. K., 1984, "Far-Field Thermomechanical Analyses of 57 and 90 kW/Acre Spent Fuel Repositories in the Topopah Spring Member of Yucca Mountain, Nevada Test Site," RE/SPEC Topical Report RSI-0232, p. 28-31, 47-50.
- Sykes, M. L., G. H. Heiken, and J. R. Smyth, 1979, "Mineralogy and Petrology of Tuff Units from the UE25a-1 Drill Site, Yucca Mountain, Nevada," Los Alamos National Laboratory Report LA-8139-MS, 76 pp.
- Tardy, Y., and J.-P. Cassan, 1981, "Hypothese Sur la Circulation Convective des Fluides de la Diagenese. Mineralogie et Petrologie des Reservoirs Greseux de l'Infrasalifere due Gabon," Compt. Rend. Acad. Sci. Paris, 293 (Ser. II):587-591.

- U.S. Department of Energy, 1984, "General Guidelines for the Recommendation of Sites for Nuclear Waste Repositories," 10 CFR 960, July 3, 1984.
- van Lier, J. A., P. L. de Bruyn, and J. Th. G. Overbeek, 1960, "The Solubility of Quartz," Jour. Phys. Chem. 64:1675-1682.
- Volosov, A. G., I. L. Khodakovsky, and B. N. Ryzhenko, 1972, "Equilibria in the System $\text{SiO}_2\text{-H}_2\text{O}$ at Elevated Temperatures Along the Lower Three-Phase Curve," Geokhimiya 5:575-591.
- Walther, J. V., and H. C. Helgeson, 1977, "Calculation of the Thermodynamic Properties of Aqueous Silica and the Solubility of Quartz and its Polymorphs at High Pressures and Temperatures," Amer. Jour. Sci. 277:1315-1351.
- Willey, J. D., 1980, "Effects of Aging on Silica Solubility: A Laboratory Study," Geochem. Cosmochem. Acta. 44:573-578.
- Wollast, R., 1967, "Kinetics of Alteration of K-feldspar in Buffered Solutions at Low Temperature," Geochem. Cosmochem. Acta. 31:635-648.

DISTRIBUTION LIST

B. C. Rusche (RW-1)
Director
Office of Civilian Radioactive
Waste Management
U.S. Department of Energy
Forrestal Building
Washington, DC 20585

J. W. Bennett (RW-20)
Office of Geologic Repositories
U.S. Department of Energy
Washington, D.C. 20545

Ralph Stein (RW-23)
Office of Geologic Repositories
U.S. Department of Energy
Washington, D.C. 20545

J. J. Fiore, (RW-22)
Program Management Division
Office of Geologic Repositories
U.S. Department of Energy
Washington, D.C. 20545

M. W. Frei (RW-23)
Engineering & Licensing Division
Office of Geologic Repositories
U.S. Department of Energy
Washington, D.C. 20545

E. S. Burton (RW-25)
Siting Division
Office of Geologic Repositories
U.S. Department of Energy
Forrestal Building
Washington, D.C. 20585

C. R. Cooley (RW-24)
Geosciences & Technology Division
Office of Geologic Repositories
U.S. Department of Energy
Washington, D.C. 20545

T. P. Longo (RW-25)
Program Management Division
Office of Geologic Repositories
U.S. Department of Energy
Washington, DC 20545

Cy Klingsberg (RW-24)
Geosciences and Technology Division
Geologic Repository Deployment
U. S. Department of Energy
Washington, D. C. 20545

B. G. Gale (RW-25)
Siting Division
Office of Geologic Repositories
U.S. Department of Energy
Forrestal Building
Washington, D.C. 20585

R. J. Blaney (RW-22)
Program Management Division
Office of Geologic Repositories
U.S. Department of Energy
Washington, D.C. 20545

R. W. Gale (RW-44)
Outreach Division
Office of Geologic Repositories
U.S. Department of Energy
Forrestal Building
Washington, D.C. 20585

J. E. Shaheen (RW-44)
Institutional Relations Staff
Office of Geologic Repositories
U.S. Department of Energy
Forrestal Building
Washington, D.C. 20585

J. O. Neff
Salt Repository Project Office
U.S. Department of Energy
505 King Avenue
Columbus, OH 43201

D. C. Newton (RW-23)
Engineering & Licensing Division
Office of Geologic Repositories
U.S. Department of Energy
Washington, D.C. 20545

S. A. Mann, Manager
Crystalline Rock Project Office
U.S. Department of Energy
9800 South Cass Avenue
Argonne, IL 60439

O. L. Olson, Project Manager
Basalt Waste Isolation Project Office
U.S. Department of Energy
Richland Operations Office
Post Office Box 550
Richland, WA 99352

K. Street, Jr.
Lawrence Livermore National
Laboratory
Post Office Box 808
Mail Stop L-209
Livermore, CA 94550

D. L. Vieth, Director (4)
Waste Management Project Office
U.S. Department of Energy
Post Office Box 14100
Las Vegas, NV 89114

L. D. Ramspott (3)
Technical Project Officer for NNWSI
Lawrence Livermore National
Laboratory
P.O. Box 808
Mail Stop L-204
Livermore, CA 94550

D. F. Miller, Director
Office of Public Affairs
U.S. Department of Energy
Post Office Box 14100
Las Vegas, NV 89114

D. C. Hoffman
Los Alamos National Laboratory
P.O. Box 1663
Mail Stop E-515
Los Alamos, NM 87545

D. A. Nowack (14)
Office of Public Affairs
U.S. Department of Energy
Post Office Box 14100
Las Vegas, NV 89114

D. T. Oakley (3)
Technical Project Officer for NNWSI
Los Alamos National Laboratory
P.O. Box 1663
Mail Stop F-671
Los Alamos, NM 87545

B. W. Church, Director
Health Physics Division
U.S. Department of Energy
Post Office Box 14100
Las Vegas, NV 89114

W. W. Dudley, Jr. (3)
Technical Project Officer for NNWSI
U.S. Geological Survey
Post Office Box 25046
418 Federal Center
Denver, CO 80225

Chief, Repository Projects Branch
Division of Waste Management
U.S. Nuclear Regulatory Commission
Washington, D.C. 20555

NTS Section Leader
Repository Project Branch
Division of Waste Management
U.S. Nuclear Regulatory Commission
Washington, D.C. 20555

Document Control Center
Division of Waste Management
U.S. Nuclear Regulatory Commission
Washington, D.C. 20555

V. M. Glanzman
U.S. Geological Survey
Post Office Box 25046
913 Federal Center
Denver, CO 80225

P. T. Prestholt
NRC Site Representative
1050 East Flamingo Road
Suite 319
Las Vegas, NV 89109

J. B. Wright
Technical Project Officer for NNWSI
Westinghouse Electric Corporation
Waste Technology Services Division
Nevada Operations
Post Office Box 708
Mail Stop 703
Mercury, NV 89023

M. E. Spaeth
Technical Project Officer for NNWSI
Science Applications, Inc.
2769 South Highland Drive
Las Vegas, NV 89109

ONWI Library (2)
Battelle Columbus Laboratory
Office of Nuclear Waste Isolation
505 King Avenue
Columbus, OH 43201

SAI-T&MSS Library (2)
Science Applications, Inc.
2950 South Highland Drive
Las Vegas, NV 89109

W. M. Hewitt, Program Manager
Roy F. Weston, Inc.
2301 Research Blvd., 3rd Floor
Rockville, MD 20850

W. S. Twenhofel
820 Estes Street
Lakewood, CO 80215

H. D. Cunningham
General Manager
Reynolds Electrical &
Engineering Co., Inc.
P.O. Box 14400
Mail Stop 555
Las Vegas, NV 89114

A. E. Gurrola
General Manager
Energy Support Division
Holmes & Narver, Inc.
Post Office Box 14340
Las Vegas, NV 89114

T. Hay, Executive Assistant
Office of the Governor
State of Nevada
Capitol Complex
Carson City, NV 89710

J. A. Cross, Manager
Las Vegas Branch
Fenix & Scisson, Inc.
Post Office Box 15408
Las Vegas, NV 89114

R. R. Loux, Jr., Manager (8)
Nuclear Waste Project Office
State of Nevada
Capitol Complex
Carson City, NV 89710

N. E. Carter
Battelle Columbus Laboratory
Office of Nuclear Waste Isolation
505 King Avenue
Columbus, OH 43201

C. H. Johnson
Nuclear Waste Project Office
State of Nevada
Capitol Complex
Carson City, NV 89710

John Fordham
Desert Research Institute
Water Resources Center
P.O. Box 60220
Reno, NV 89506

Dr. Martin Mifflin
Desert Research Institute
Water Resources Center
Suite 201
1500 East Tropicana Avenue
Las Vegas, NV 89109

J. L. Younker (25)
Science Applications, Inc.
2769 S. Highland Drive
Las Vegas, NV 89101

Karsten Pruess
Earth Sciences Division
Lawrence Berkeley Laboratory
University of California
Berkeley, CA 94720

6300 R. W. Lynch
6310 T. O. Hunter
6311 L. W. Scully
6311 L. Perrine (2)
6312 F. W. Bingham
6312 J. W. Braithwaite (10)
6312 T. S. Ortiz
6312 R. R. Peters
6312 S. Sinnock
6312 M. S. Tierney
6313 J. R. Tillerson
6313 J. A. Fernandez
6313 E. A. Klavetter
6313 F. B. Nimick (10)
6330 G. R. Romero
6330 NNWSICF
3141 C. M. Ostrander (5)
3151 W. L. Garner (3)
8424 M. A. Pound